UNIVERSITI
MALAYSIA
KELANTAN

Effect of Groove Shape to the Mechanical Properties in Gas Metal Arc Welding Process

Choo Jia Xin
J20A0659

A reported submitted in fulfilment of the requirements for the degree of Bachelor of Applied Science (Material Technology) with Honours

FACULTY OF BIOENGINEERING AND TECHNOLOGY
UMK

2023

DECLARATION

I declare that this thesis entitled "Effect of Groove Shape to the Mechanical Properties in Gas Metal Arc Welding Process" is the results of my own research except as cited in the references.

Signature : 

Student's Name : CHOO JIA XIN

Date : 28th February 2024

Verified by:

Signature :

Supervisor's Name : ASSOC. PROF. TS. DR. SARIZAM BIN MAMAT

Stamp:

Date:

ACKNOWLEDGEMENT

This work would not have been possible without the support and facilities provided by Faculty of Bioengineering and Technology at University Malaysia Kelantan. I am indebted to my supervisor, Assoc. Prof. Ts. Dr. Sarizam Bin Mamat who has been continuously guiding and supporting me along the whole journey of my final year project. Learning under his guidance, I acquired the research methodology and the skill to present my work with utmost clarity. It was a profound privilege and honor to be under his mentorship while working and studying.

Furthermore, I am sincerely grateful to the laboratory assistants of Faculty of Bioengineering and Technology at University Malaysia Kelantan for their continuous assistance and guidance throughout my laboratory work and analysis procedures. I wish to express my appreciation to all the laboratory assistants that were involved along the way. They played a crucial role in supporting and facilitating the completion of my final year project, without their help I wouldn't be able to fulfil and finish my final year project.

Moreover, to all my dearest fellow friends who never give up in giving me support, valuable information and assisted me in completing this study. A word of thanks also extends to those who have indirectly provided comments and helpful suggestions.

Finally, my deepest appreciation to my family for consistently providing mental support and motivation throughout this final year project. Thank you for always being so supportive and helping me every step of the way.

Effect of Groove Shape to the Mechanical Properties in Gas Metal Arc Welding Process

ABSTRACT

Mild steel is a material commonly used in various industrial applications. Mild steel is classified as low carbon steel, has a carbon concentration ranging from 0.16 to 0.29 wt% and melts between 1450 to 1520°C. Gas metal arc welding (GMAW) is widely utilized in various industries due to its numerous advantages. Welding parameters plays a crucial role in ensuring high quality welds. Generally, welding parameters including current, voltage, arc length, contact tip to work distance (CTWD), travel and work angle, welding speed and size of electrode. Groove shape and type of joining in welding also significant influence the mechanical properties of welded joint. The objectives of this final year project are to study the effect of groove shape to the microstructure formation behaviour at weld metal and heat affected zone and to investigate the influence of groove shape on mechanical properties in both single and multi-layer welded joints. In this study, single and multi-layer welding were employed to prepare butt weld joints using V and U grooves in the specimens. The metallographic studies of samples subjected to Nital etching and Le Pera etching were carried out using optical microscopy were proven the influence of groove shape on microstructure and consequential impact on mechanical properties. The evaluation of mechanical properties of samples was conducted using Vicker Hardness Tester and Charpy Impact Tester. Vicker hardness results showed that single layer welding of U groove (SU) exhibited higher hardness than single layer welding of V groove (SV) and in multi-layer welding of V groove (MV) exhibited higher hardness than U groove (MU). Charpy impact test was conducted at three different temperatures (20°C, 0°C and -20°C). For single layer welding, the results showed that no significant difference for both V and U groove tested at 20°C. However, SU showed high impact toughness compared to SV at 0°C while SV slightly advantage SU at -20°C. For multi-layer welding, MV showed high impact toughness across both room temperature and 0°C. However, MU exhibited better impact toughness at -20°C compared to MV.

Keywords: GMAW, Low Carbon Steel, Butt Joint, Groove Shape

Kesan Bentuk Alur Terhadap Sifat Mekanikal dalam Proses Kimpalan Arka Logam

ABSTRAK

Keluli lembut merupakan bahan yang biasa digunakan dalam pelbagai aplikasi industri. Keluli lembut diklasifikasikan sebagai keluli karbon rendah, dengan kepekatan karbon berkisar antara 0.16 hingga 0.29 wt% dan melebur antara 1450 hingga 1520°C. Pengimpal elektrik gas logam (GMAW) banyak digunakan dalam pelbagai industri kerana kelebihannya yang banyak. Parameter pengimpalan memainkan peranan penting dalam memastikan kualiti tinggi pada sambungan las. Secara umum, parameter pengimpalan termasuk arus, voltan, panjang arus, jarak mata sentuh ke kerja (CTWD), perjalanan dan sudut kerja, kelajuan pengimpalan, dan saiz elektrod. Bentuk alur dan jenis penyambungan dalam pengimpalan juga mempengaruhi sifat mekanikal sambungan las. Objektif projek tahun akhir ini adalah untuk mengkaji kesan bentuk alur terhadap tingkah laku pembentukan mikrostruktur di logam las dan zon terkena panas serta menyiasat pengaruh bentuk alur ke atas sifat mekanikal dalam penyambungan las tunggal dan pelbagai lapisan. Dalam kajian ini, pengimpalan lapisan tunggal dan pelapisan berganda digunakan untuk menyediakan sambungan las bertompok menggunakan alur V dan U pada spesimen. Kajian metalografi terhadap sampel yang telah dikenakan etsa Nital dan etsa Le Pera menggunakan mikroskopi optik telah membuktikan pengaruh bentuk alur terhadap mikrostruktur dan kesan seterusnya terhadap sifat mekanikal. Penilaian sifat mekanikal sampel dijalankan menggunakan Penyahpejal Kekerasan Vicker dan Ujian Impak Charpy. Keputusan kekerasan Vicker menunjukkan bahawa penyambungan las tunggal alur U (SU) menunjukkan kekerasan yang lebih tinggi berbanding penyambungan las tunggal alur V (SV), dan dalam penyambungan las pelbagai lapisan alur V (MV) menunjukkan kekerasan yang lebih tinggi berbanding alur U (MU). Ujian impak Charpy dijalankan pada tiga suhu berbeza (20°C, 0°C dan -20°C). Untuk pengimpalan lapisan tunggal, keputusan menunjukkan tiada perbezaan yang signifikan untuk kedua-dua alur V dan U diuji pada 20°C. Walau bagaimanapun, SU menunjukkan ketangguhan impak yang tinggi berbanding SV pada 0°C manakala SV sedikit lebih unggul daripada SU pada -20°C. Bagi pengimpalan lapisan berganda, MV menunjukkan ketangguhan impak yang tinggi di kedua-dua suhu bilik dan 0°C. Walau bagaimanapun, MU menunjukkan ketangguhan impak yang lebih baik pada -20°C berbanding dengan MV.

Kata kunci: GMAW, Keluli Karbon Rendah, Sambungan Bertompok, Bentuk Alur

TABLE OF CONTENTS

LIST OF TABLES

LIST OF FIGURES

CHAPTER 1

INTRODUCTION

1.1 Background of Study

Mild steel is a material commonly used in various industrial applications. It is an economical type of steel with a carbon concentration ranging from 0.16 to 0.29 wt% and its melting temperature is in a range of 1450 to 1520°C. Its melting point is higher compared to other grade of steels that contain higher levels of carbon, primarily due to its lower carbon content (Sarkari Khorrami et al., 2014). However, there were still significant drawbacks due to mild steel experienced fatigue failure when subjected to cyclic loading over time (Aldeeb et al., 2018). As a result, structures that made from mild steel may leads to fracture. Additionally, due to mild steel has a relatively low tensile strength, it is not an ideal for application requiring high strength-to-weight ratios or impact resistance. Despite its drawbacks, mild steel continues to be widely utilized in welding applications due to its advantageous properties.

Welding is a process of joining two or more materials at their contacting surfaces by applying heat to form one piece (Olabode et al., 2013). The four primary basic welding methods includes shielded metal arc welding (SMAW), gas tungsten arc welding (GTAW), gas metal arc welding (GMAW) and flux-cored arc welding (FCAW). In comparison, GMAW is extensively employed across various industries owing to its numerous advantages.

GMAW which known as a welding technique that involves continuous feeding of solid wire under a shielding gas to ensure a protective welding environment. The purpose of

employing shielding gas during welding is to protect the weld pool and prevent any contamination that would affect the overall performance of final products (Mvola & Kah, 2017). During welding, an arc is generated between the wire tip and the workpiece intended for welding. The constant feeding of the wire allows the creation of longer welds without interruption. GMAW welding process is characterized by relatively high deposition rate compares to shielded metal arc welding (SMAW) (Posch & Welding, 2014). This is due to SMAW involves heating metals using an electric arc to provide shielding between a coated electrode and the workpiece (Singh et al., 2019). This result with less effectiveness in preventing contamination and directly decrease the deposition rate. However, compare to GMAW which uses an external shielding gas such as Argon (Ar) to prevent atmospheric contamination and thus result with high deposition rate. Moreover, compared to other welding methods, it provides a comparatively low heat input.

Welding parameters plays a crucial role in ensuring high quality welds. Generally, welding parameters including current, voltage, arc length, contact tip to work distance (CTWD), travel and work angle, welding speed and size of electrode. Throughout the welding process, there were some parameters that required consideration such as heat input, bead shape, weld penetration, microstructure properties and more. The interaction of the heat source and the welding specimen can be divided into four distinct regions namely the weld metal, Transition Zone, Heat Affected Zone (HAZ) and Unaffected Base Metal Zone (Śloderbach & Pajak, 2015).

According to the research conducted by Sultana et al. (2014), the mechanical properties of mild steel were affected by heat treatment and indirectly impacted on the mechanical properties. Considering these facts, the application of different groove shapes was considered to address the issues as the groove shape in welding had a significant impact on the mechanical properties and microstructure of the welded joint. The amount and distribution

of the weld metal, the heat input during welding and the stress distribution in the joint were all influenced by the groove shape (Ye et al., 2015). Therefore, it is important that proper selection of input process parameters and control on the weld bead shape is necessary to achieve the desired weld bead shape (Sarolkar & Kolhe, 2017). In this study, single-v and single-u grooves were used to prepare butt weld joints in the specimens. Based on Figure 1.1, butt welding was a process that was used to join a part that were nearly parallel and had no overlap with each other. When performing butt welding, the standard procedure involves heating up the two weld ends using a weld plate and then joining them together under a specific pressure.

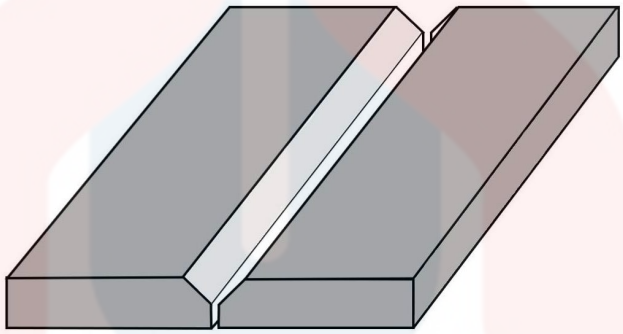

Figure 1. 1: Butt Joint

During welding process, a localized heat is introduced to the specimen at a concentrated point to form a proper weld by applying the high-energy density heat source (Singh, 2020). GMAW commonly known as metal inert gas (MIG) is an arc welding process. In the process of arc welding, heat input (HI) refers to the total energy supplied to the workpiece to create a weld. Units of energy per unit length were used to measure HI and heat represent the energy outage that had been produced.

$$Heat\ input, H = \frac{Ampere\ \times Volts}{Travel\ speed, v}$$

Unit = J/mm

where:

I is the current used, in amperes

V is the voltage used, in volts

v is the travel speed of the welding torch, in mm per second (mms^{-1})

Basically, the overall heat contribution required depended on the thickness, welding speed and joint type. Proper adjusting the heat input according to the factors is crucial for a reliable weld.

1.2 Problem Statement

The ability of mild steel to resist tension is a crucial aspect that determines its mechanical characteristics and its appropriateness for different uses (Elfallah, 2022). The shape of the groove in a mild steel specimen can impact its tensile strength due to the creation of a stress concentration point which makes the material more vulnerable to failure. However, more research was required to comprehend the impact of distinct groove shapes on the tensile strength of mild steel since the extent and nature of this impact were not well understood. Additionally, the mechanical properties of mild steel can be influenced by the grain size present in its microstructure through optical microscopy. It was reported that characterizing the complicated melt-pool behaviour, which exhibits highly non-linear reactions to change in process parameters is one of the challenges for the development, qualification and optimization of arc welding process (Ebrahimi et al., 2021).

Therefore, the aim of this experiment is to investigate the impact of groove shape, specifically single-v and single-u grooves on the tensile strength of butt weld joints. Throughout the research it can be provided valuable insights into the relationship between groove shape and mechanical properties, facilitating the development of mild steel structures and parts.

1.3 Objectives

The objective of this research is:

1. To study the effect of groove shape to the microstructure formation behaviour at weld metal and HAZ.
2. To investigate the influence of groove shape on mechanical properties in both single and multi-layer welded joints.

1.4 Scope of Study

The scope of the study is conducted to achieve and support the objective mentioned. This research was conducted in University Malaysia Kelantan. In this research, the raw materials for the preparation of distinct groove shapes on the mechanical properties in gas metal arc welding (GMAW) including specimens of mild steel in a specific size and shape were properly prepared. The mild steel specimens of a defined dimension were cut to create precise groove shapes which were single-v and single-u grooves. The butt joint weld method was used to join two pieces of mild steel together. Once the welding process was complete, the welded joint undergo inspection and testing to evaluate its strength and other mechanical properties. Qualitative tests were done following the optical microscopy techniques and quantitative method were performed using the Charpy Impact Tester. Lastly, the collected data was used to determine the impact energy and fracture characteristics.

1.5 Significances of Study

The research aims to evaluate the mechanical properties of mild steel specimens by using distinct groove shapes. Distinct groove shapes of mild steel especially single-v groove

have showed potentials to be used in many applications due to its strong joint and suitable for a variety of structural and load-bearing applications. This study also served as a reference for future research.

CHAPTER 2

LITERATURE REVIEW

2.1 Welding Mild Steel

Mild steel is also known as low carbon steel which has less than 0.25% of carbon content (Evans, 2012). The industrial sector commonly selects mild steel due to its physical properties such as high tensile strength, good weldability and ductility. According to Khamari et al. (2020), the need for advancements in materials joining is critical due to the increased demand for production, construction and various engineering. Therefore, proper welding of mild steel is important to meet the required specifications and standards.

2.2 Groove Shape in GMAW

When it comes to metal manufacturing industry, mechanical properties are a significant factor in determining the appropriate metal for each specific task. The main concern being addressed is the potential impact of groove shape on the mechanical properties of a welded joint produced by the GMAW. Groove shape refers to the design or configuration of the groove that use in welding. The mechanical properties of the welded metal were influenced by variations in welding parameters caused by different groove shapes. According to Sattari-Far and Farahani (2009), it is important to mention that most published studies only focus on welding joints with a V-groove shape. Therefore, further investigation and

experimentation need to be carried out to fully understand the impact of distinct groove shape on the mechanical properties in GMAW.

2.3 Weld Geometry

In this section, the types of welds joint, weld grooves and weld pass for mechanical properties purposes were reviewed.

2.3.1 Weld Joint

Welding is the process of joining two metal pieces together to create a single piece by heating the metals to their melting points. Based on Figure 2.1 butt joint, lap joint, T-joint, edge joint and corner joint are typical welding joint types (Zaidi & Madavi, 2018). Basically, joint design was influenced by material thickness and types of alloy used in welding (Olabode et al., 2013).

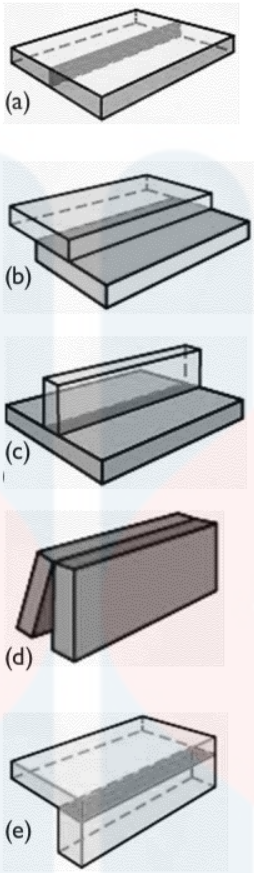

Figure 2. 1: Types of joints (a) butt joint (b) lap joint (c) T-joint (d) edge joint (e) corner joint (Source: Olabode et al., 2013)

Previous research done by Winarto et al. (2018) on the strength of steel using butt and fillet joint in GMAW has shown that hardness of heat affected zone (HAZ) and weld metal (WM) near the bottom surface is greater compared to upper surface in butt weld joint. Since butt joint provides strong and reliable connections, it is more suitable to apply in this final year project compared to other types of joints.

2.3.2 Weld Groove

Weld groove refers to the shape of joint area where welding take place. Basic types of weld groove include j-groove, u-groove, v-groove and more. There were several factors influenced by the design of the weld groove and one of them is strength. From the previous research carried out by Elfallah (2022) regarding on the influence of groove shape on the

tensile strength of commercial steel discovered that V-groove welding had a higher impact on the tensile strength and hardness of the weld in GMAW.

2.3.3 Weld Pass and Weld Layer

In welding, careful consideration of weld passes and weld layers is important to contribute to the formation of a complete weld. Weld pass is a single traversal along the joint while weld layer is the material deposited in a single pass. Denoting that multiple weld passes are made to create multiple weld layers. According to (Moon et al., 2006), there are three different types of passes and different terms are used to refer the weld passes deposited at various stages of a multi pass weld. These three passes are namely root pass, fill pass and cap pass. In this final year project, both single pass welding with a single layer and multi pass welding involving three layers will be conducted.

2.4 Gas Metal Arc Welding (GMAW)

Gas Metal Arc Welding (GMAW) was used in this final year project to join the workpiece together. GMAW is welding where an electric arc consolidates with continuous-feed wire filler shielded with shielding gas for generating heat (Naidu et al., 2003). GMAW is also categorized as Metal Inert Gas (MIG) welding and according to Elfallah (2022), shielding gases can be either inert such as argon or helium or active such as carbon dioxide and oxygen.

2.4.1 Major Challenges of GMAW

According to Kah and Martikainen (2012), welding industry faces a few significant challenges due to the need for increase productivity, efficiency and quality. Major challenges

of GMAW to get a weld with superior quality is welding parameters. Current, voltage, travel speed, arc length and other variables were among them. In general, proper operational skills of welding are essential to achieve high-quality welds with minimal defects. Although there are other types of welding such as shielded metal arc welding (SMAW), gas tungsten arc welding (GTAW), flux-cored arc-welding (FCAW) but only GMAW meets the requirement of the final year project due to its adjustable parameters and high deposition rates.

2.5 GMAW Techniques

In this section, welding techniques were reviewed to achieve high quality welds at the same time ensure both the welder's safety and the final product.

2.5.1 Basic Parameters of Welding

Parameters of welding can be divided into two categories which are variable parameters and fixed parameters. Variable parameters refer to the changeable factors that can be adjust during the welding process to achieve expected outcome. This including current, voltage, heat input and etc. Conversely, fixed parameters refer to the predetermined factors that remain consistent throughout the welding process. This including base material thickness, joint design etc. In this final year project, the focus will be on analysing and optimizing the welding process by manipulating key variables parameters while also considering fixed parameters.

2.6 Non-Destructive Testing (NDT) of Weld

Non-destructive testing (NDT) is a technique that use to test a material without causing any damage or destruction to it (Deepak et al., 2021). In this research, NDT such as visual appearance observation and microstructure observation were reviewed.

2.6.1 Visual Appearance Observation

According to Ghazvinloo et al. (2021), visual testing was carried out by examined the top surface and cross section of all welded joints with naked eye to identify any present of flaws. In this final year project, this method will be used to inspect the weld toe angle, reinforcement height, penetration depth, weld bead size and heat-affected zone (HAZ) size.

2.6.2 Microstructure Observation

Microstructure observation refers to the examination and analysis of the structural and compositional characteristics of materials under a microscope. The observation can be carried out by using optical microscope (OM) and scanning electron microscope (SEM). OM was utilized to examine the microstructures of the weld, HAZ and any variation. Meanwhile, SEM was utilized to determine the type of fracture that occurred during mechanical testing of the joints (Sharma & Shahi, 2014).

According to Winarto et al. (2018), Figure 2.2 has shown the macrograph of butt joint under optical microscope and the study was found that width of HAZ is about 2mm. On the other hand, it has reported that the HY-80 steel microstructure of base metal and HAZ consisted of a combination of granular bainite (GB), ferrite (F) and martensite (M) while the weld metal exhibited acicular ferrite (AF) (Figure 2.3).

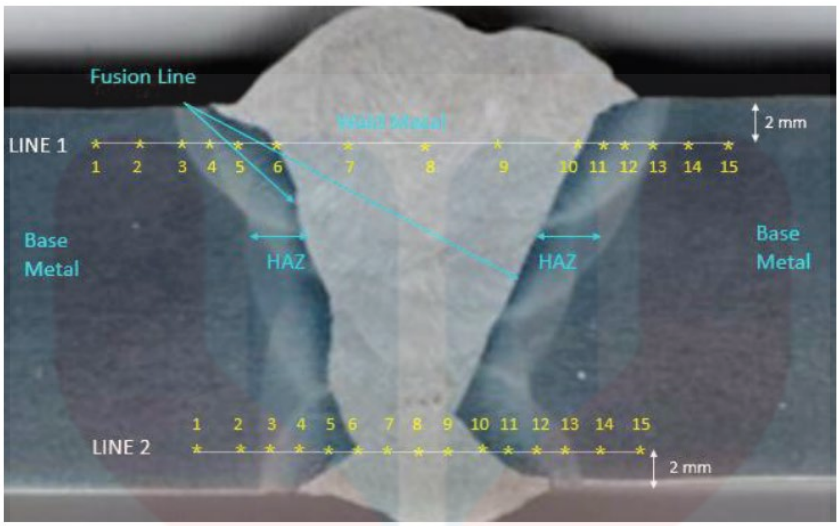

Figure 2. 2: Macrograph of butt joint under OM

(Source: Winarto et al., 2018)

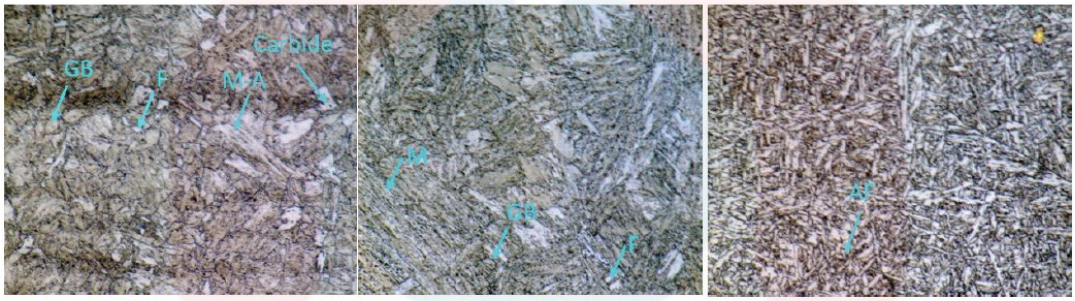

Figure 2. 3: Micrograph of butt joint under OM with 1000X magnification (a) base metal (b) Heat affected zone (c) Weld metal

(Source: Winarto et al., 2018)

The findings of this study regarding the base metal exhibit similarities to the outcomes reported by Sharma and Shahi (2014). From the observation under 2000X magnification with SEM, the presence of distinct grains of lath martensite separated by high angle boundaries in quenched and tempered low alloy abrasion resistant steel (Figure 2.4). At the same time, the WM exhibited mainly acicular ferrite (ACF), ferrite with a secondary phase (FS) and grain boundary ferrite (GBF).

In the field of scientific imaging, optical and scanning electron microscopes are commonly used. Despite both instruments serving the purpose of characterizing microscopic

samples, however OM are typically easier to operate and require less specialized training compared to SEM which demands more expertise and experience due to its complex nature. In this case, optical microscope will be used as the microstructure analysis for this final year project because of its convenience and suitability.

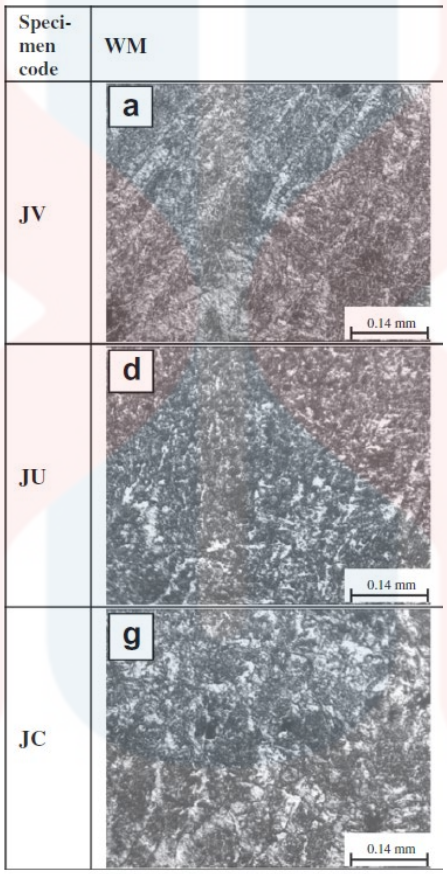

Figure 2. 4: Micrograph of butt joint weld metal with three different grooves under SEM with 2000X magnification

(Source: Sharma & Shahi, 2014)

2.6.3 Measurement of Welding Dilution Rate

Dilution is the mixing of base metal with the filler metal during welding process. Based on figure 2.5, measurement of dilution rate includes bead width, bead height and penetration (Anis et al., 2017). Additionally, dilution rate will be influenced by various welding parameters such as welding speed, current, voltage etc. According to Kumar Gupta et

al. (2019), the dilution rate is calculated as the ratio of fused base metal to the volume of total weld deposit. The dilution rate (%) will be calculated as follows.

$$Dilution\ Rate\ (\%) = \frac{A + C}{A + B + C} \times 100\%$$

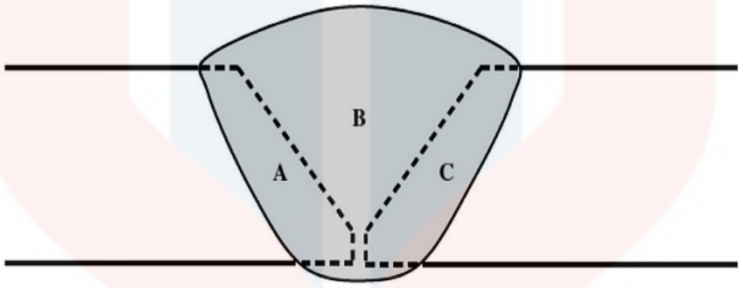

Figure 2. 5: Schematic diagram of dilution rate measurement

(Source: Anis et al., 2017)

2.7 Destructive Testing (DT) of Weld

Conversely, destructive testing (DT) is a technique that use to evaluate the properties and behaviours of a material by altering or damaging the material. In this research, DT of mechanical testing includes hardness testing, impact testing and tensile testing were reviewed.

2.7.1 Mechanical Testing

From the previous research carried out by Sharma and Shahi (2014)regarding the mechanical and metallurgical properties of welded joints in quenched and tempered low alloy abrasion-resistant steel were influenced by the design of the groove. The mechanical properties of the material including toughness, microhardness and tensile strength were examined in this study using a Charpy impact tester, Vickers hardness tester and Universal Tensile machine respectively.

According to ASTM E23 charpy impact test standard, samples are prepared with dimensions of length 55mm, width 10mm and thickness 10mm. This test is used to determine the toughness of welded samples. Followed by Vickers hardness test which is a microhardness test method to determine the hardness of welded samples. According to (Kumar et al., 2017), the preparation of sample sizes for the Vickers hardness test follows standard dimensions of length 30mm, width 6mm and thickness 6mm. On the other hand, tensile test is used to determine the material's mechanical properties under tension. UTM typically require specific sample shapes such as dumbbell shape for conduct tensile test. However, the samples presented difficulties in preparing the prescribed shapes. Thus, charpy impact tester and Vickers hardness tester will be used to evaluate the mechanical properties in this final year project because of its convenience and suitability in this current condition.

CHAPTER 3

MATERIALS AND METHODS

3.1 Flowcharts

Figure 3.1 shows the process of sample preparations, metallographic studies and mechanical testing for evaluate the microstructure and mechanical properties of welded joints with V and U groove configurations.

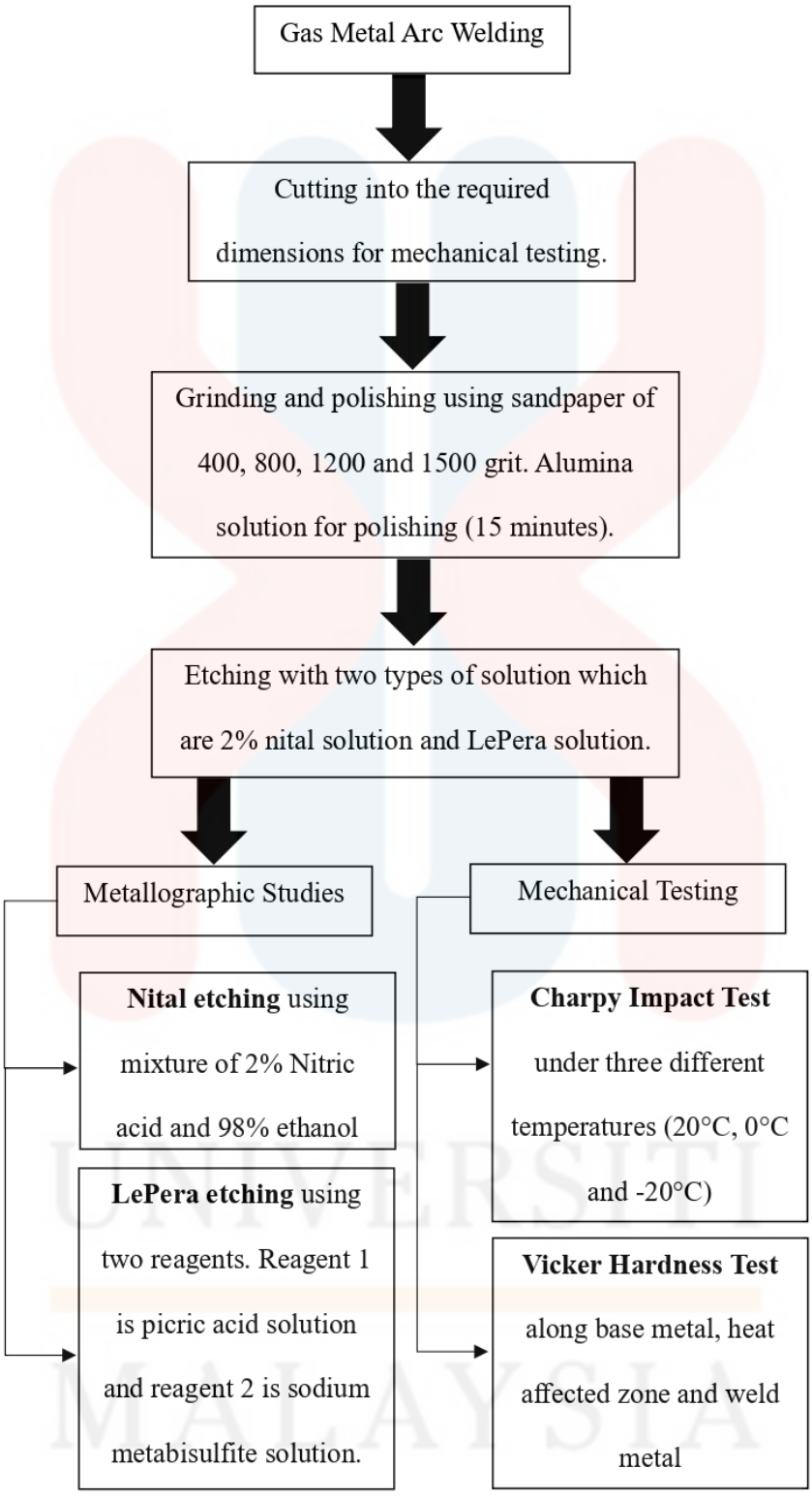

Figure 3. 1: Flowchart of experimental procedures

3.2 Welding Process

The process of welding the base metal was explained and the type of joint used for welding was butt joining.

3.2.1 Joint Design and Preparation

In the final year project, there were two types of groove shape namely single-V and single-U groove were used to observe the effect of distinct groove shape on the mechanical properties in GMAW. Based on the figure 3.2, a single-v groove has a geometry with two slopping sides while for figure 3.3 single-u groove has a geometry with two j-shaped cuts forming a curve.

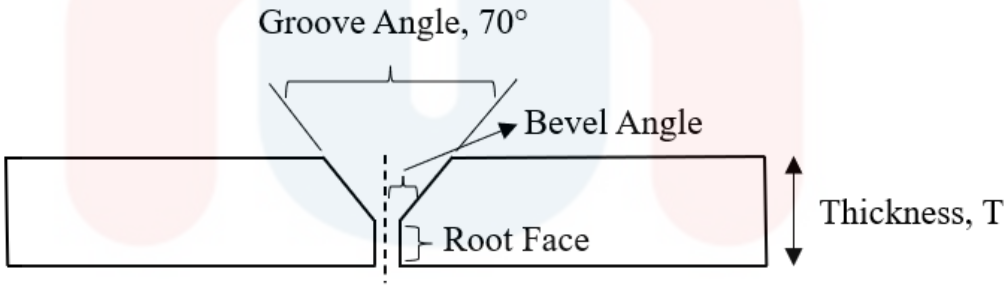

Figure 3. 2: Schematic diagram of Single-V Groove

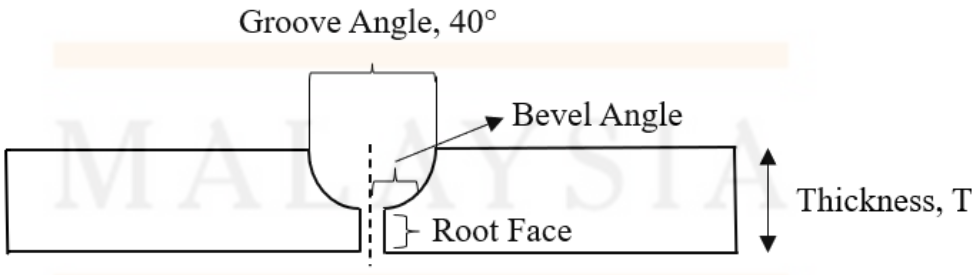

Figure 3. 3: Schematic diagram of Single-U Groove

According to Sharma and Shahi (2014), dimension of base metal is measured by Length x Width x Height which is 55 x 10 x 10 mm. In this case, height is the measurement of

thickness, T. The groove angle of the sample was prepared at 70° with the bevel angle of 35° for single plate (Pathak et al., 2020). According to Pathak et al. (2020), optimal groove angles simplify the welding process and enhance penetration depth in the workpiece. In this research, the groove angle for the single-V groove was set at 70°, while the groove angle for the single-U groove was 40°. Additionally, a root face of 2 mm was maintained for both groove types. Figure 3.4 provides a realistic depiction of the base metal with grooves U and V.

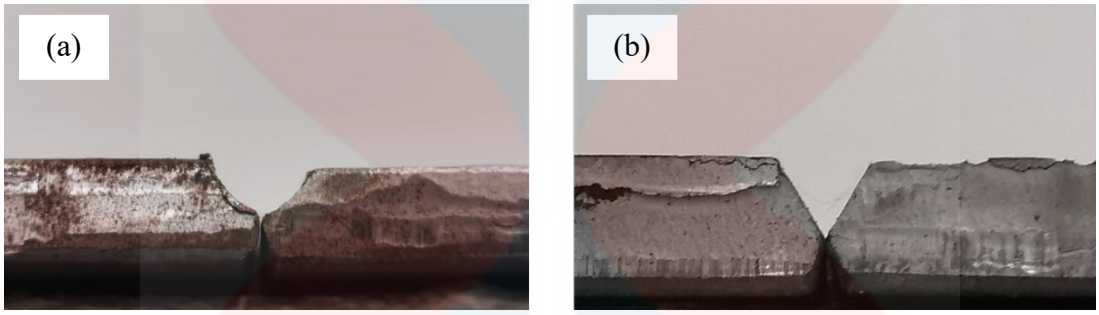

Figure 3. 4: Types of grooves in butt joint (a) U-groove (b) V-groove

3.3 Welding Parameters

The Gas Metal Arc Welding (GMAW) machine utilized in the welding process for this research is depicted in figure 3.5. The technique involved creating an electrical arc between a metal wire electrode and the welding parts to locally heat on a very high temperature. This allowed the base metal to melt and fuse together. A critical aspect of achieving desired welding outcomes lies in considering and optimizing various welding parameters.

Figure 3. 5: GMAW welding machine

Table 3.1 depicts the welding parameters employed in GMAW, encompassing condition such as the type of welding torch, electrode wire/ diameter, polarity, current, voltage, heat input, contact tip work distance, travel angle, welding speed and the use of Argon gas as the shielding gas.

Table 3. 1: The welding parameters of GMAW

Condition	**Parameter**
Welding Torch	MIG
Electrode Wire/ Diameter	ER-70s /1.0 mm
Polarity	DCEP
Current (A)	196
Voltage (V)	22
Heat Input, HI (j/mm)	862.4
Contact Tip Work Distance (mm)	12
Travel Angle	90°

Welding Speed (mm/sec)	5
Shielding Gas	Argon (Ar)

Each parameters plays a crucial role in influencing the welding process and the resulting characteristics of the weld. Polarity in welding can be categorized into alternating current (AC) and direct current (DC). DC can further divide into direct current electrode positive (DCEP) and direct current electrode negative (DCEN). According to (Mohanty et al., 2020), direct current electrode positive (DCEP) polarity enhances plate melting and produce deeper weld penetration and facilitates cleaning action by removing oxides from the weld pool. In this research, the workpiece surface was cleaned with wire brush and ethanol to remove contaminants before welding. GMAW machine was set up with DCEP for the MIG torch that contained filler wire and DCEN for the earth clamp.

In welding process, heat input (HI) is measures of how much energy has been supplied to the workpiece to form a weld. Heat input in this section was calculated using the current, voltage and welding speed. The equation was shown below.

$$Heat\ Input, H = \frac{Ampere\ \times Volts}{Travel\ Speed}$$

$$= \frac{196 \times 22}{5}$$

$$= 862.40 \text{ j/mm}$$

The experimental setup for GMAW is depicted in figure 3.6 featuring a MIG torch positioned at a 90° angle. The contact tip work distance (CTWD) is set at 12mm and welding speed at 5mm/sec. For both single layer and multi-layer V and U groove welding, the experimental setup maintains fixed parameters which shown in table 3.1 to ensure the consistency in the welding process.

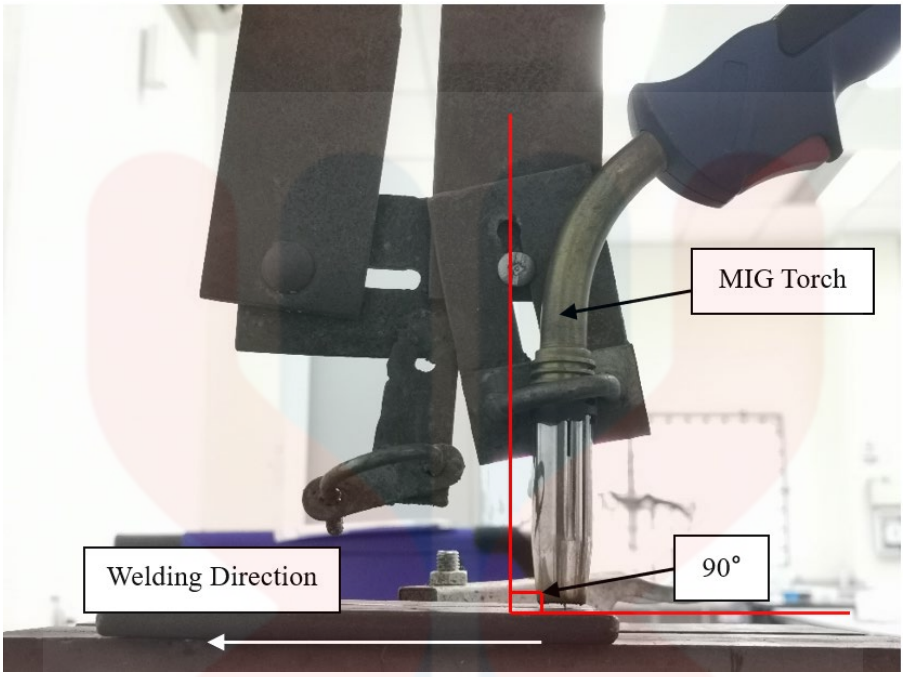

Figure 3. 6: The schematic diagram of MIG of experimental setup

3.4 Sample Preparation

Proper maintain and attend were important for the surface area that was under observation is important. In welding, sample preparation is crucial for ensuring strong weld joint integrity, clean surfaces, proper material fusion and determining appropriate welding techniques.

3.4.1 Cutting

After welding, cutting process is performed to show a cross section of butt in U and V type welding to study its microstructure. The original dimension of the mild steel plate supplied by the supplier is shown in Figure 3.7. Based on Figure 3.8, the samples were cut into dimensions of 50 mm length x 5 mm width x 5 mm thick after mild steel samples have been welded.

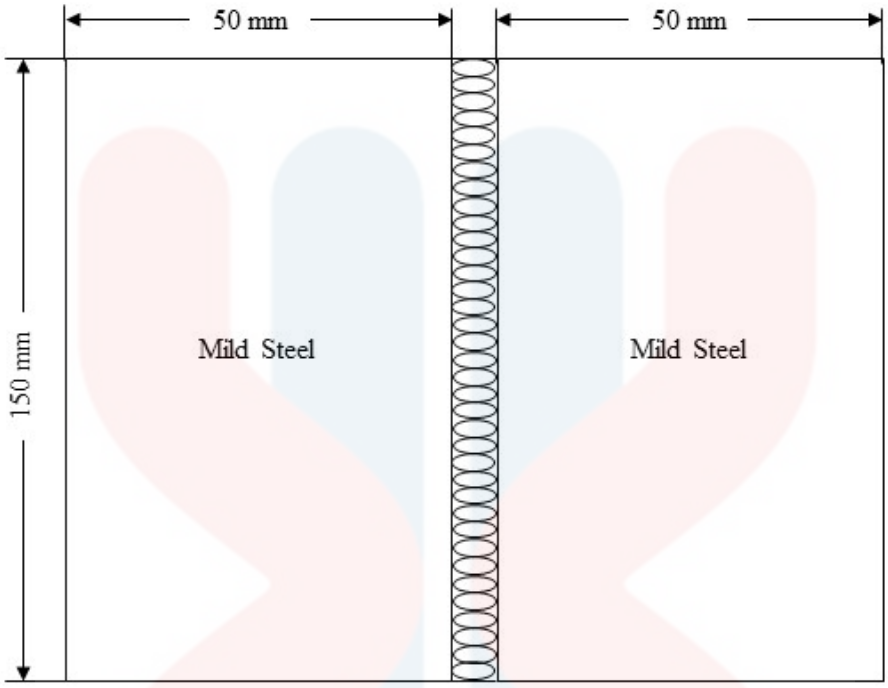

Figure 3. 7: Original dimension of mild steel plate supplied by industry

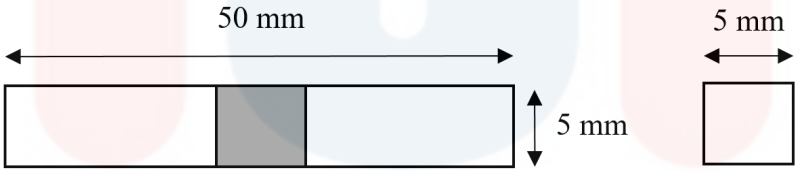

Figure 3. 8: Dimension for grinding and polishing process

3.4.2 Grinding

In grinding process, sandpaper with the grit of 400, 800, 1200 and 1500 grit was used to grind the samples precisely. The process started by using the lowest grit to the highest grit to ensure the samples were in the best condition to be polished. In this step, care must be taken to avoid being too abrasive which could potentially result in creating greater damage on the specimen. It was important to make sure the pressure applied to the sample during grinding was uniform so that the resulting surface was flat and had the same degree. The grinding process should be done in one direction only which is 90° to prevent scratches on the

surface and cause sample damage. Water was used to assist the grinding process to fasten the process.

3.4.3 Polishing

Based on figure 3.9, the MP-2B grinding/polishing machine is employed for the grinding and polishing processes. In the polishing process, liquid suspension of Alumina (Al_2O_3) and water was used until a mirror like finish was obtained. During the process, pressure applied on the samples must be even on every area to avoid any damage to the sample surface. The sample was polished in a circular motion to ensure that the polishing part turned smoother and shinier. Polishing was used to remove only surface damage.

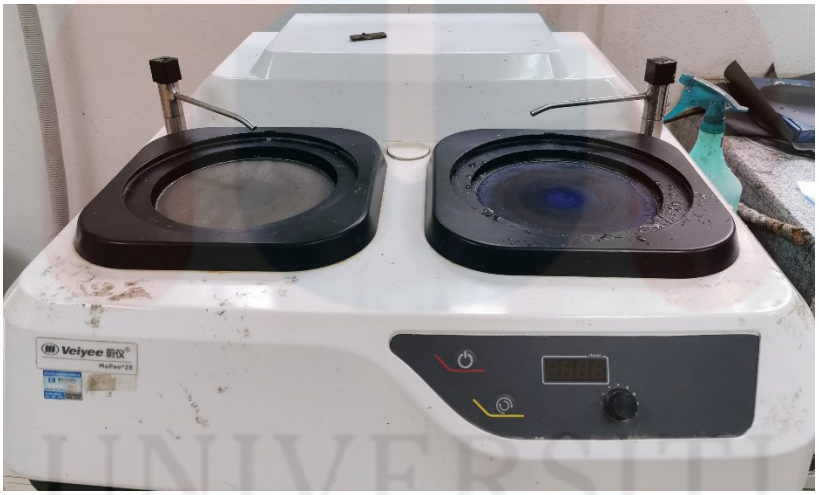

Figure 3. 9: MP-2B grinding/polishing machine

3.4.4 Sonication

Figure 3.10 shows the sonication process for welded samples of single layer and multi-layer V and U groove. Sonication is performed after polishing to remove debris and enhance cleaning by subjecting the sample to high-frequency sound waves. This process effectively cleans the surface and eliminates microscopic particles as well as helps remove contaminants like oils, greases, residues from polishing compounds through cavitation effect

by sound waves. Samples were immersed in a beaker containing ethanol (CH_3CH_2OH) then placed into Ultrasonic Bath Sonicator for approximately 5 minutes to remove alumina impurities from each sample. It's crucial to note that after sonication, each sample was thoroughly dried before proceeding to the etching step.

Figure 3. 10: Ultrasonic Bath Sonicator

3.4.5 Etching

A 2% of nital solution which contained of 2% of nitric acid and 98% of ethanol was mixed and used. Figure 3.11 (a) shows the preparation of nital solution and figure 3.11 (b) shows the process of nital etching. Etching is used to optically improve microstructural details like grain size and phase characteristics. Further etching developments made it possible to modify specific microstructural characteristics while taking into account their composition, stress levels or crystal structure. Two distinct etching techniques which are nital etching and LePera etching were employed to observe and analyse the microstructure of material under different groove shape. Both etching techniques typically reveal different microstructures when applied to a specimen. Each etching technique has its specific characteristics and

interactions with the material constituent, leading to distinct visualizations of the microstructure.

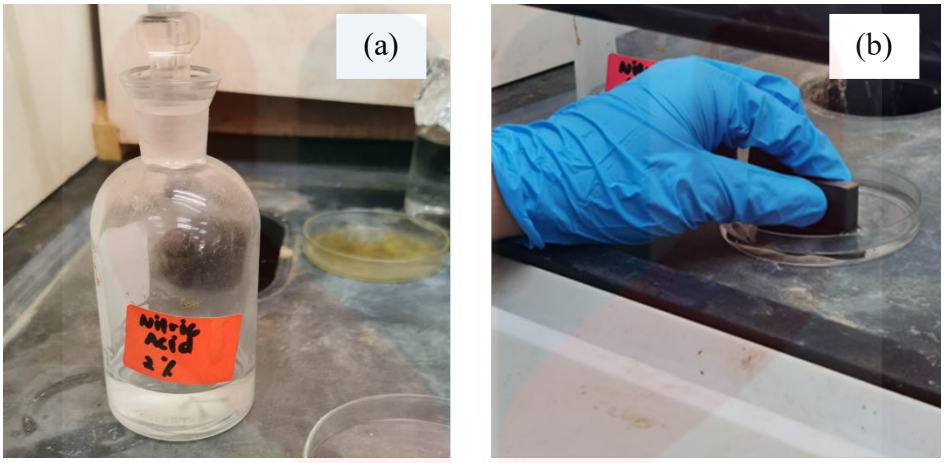

Figure 3. 11: Nital Solution (a) The preparation of Nital Solution; (b) The process of nital etching.

In nital etching, each sample underwent etching for 15 seconds, followed by rinsing with distilled water and quick drying using a hair dryer before microstructure observation. After completing the microstructure observation for nital etching, the samples were utilized to proceed with LePera etching. Polishing and sonication process was repeated to remove any residual impurities before advancing to the LePera etching stage. LePera solution was prepared with the mixture of 4 gram picric acid in 100ml ethanol for reagent 1 and 1g sodium metabisulfite in 100ml distilled water for reagent 2, in as shown in 1:1 (30ml : 30ml) volume ratio as shown in figure 3.12. LePera etchant is a mixture of two reagents which are sodium metabisulfite ($Na_2S_2O_5$) and picric acid [$(O_2N)_3C_6H_2OH$] to analyse the microstructure of the samples.

Figure 3. 12: The preparation of LePera Solution

The specimen for etching LePera solution was immersed in reagent 1 for approximately 20 seconds, followed by immersed in reagent 2 for a duration of approximately 20 seconds. The specimen was oscillated in the LePera etchant during the etching process and then it was lifted out after a few seconds to proceed to the next stage. Colour etching in metallurgy visually distinguish various phases in metals by generating specific colours for each phase, providing effective for identifying martensite and bainite (Hossein Zakerinia et al., 2009). According to Mendonça et al. (2020), LePera etching highlights martensite in bright white with retained austenite as an MA constituent, while ferrite appears in a light brown and bainite in a dark brown tone. Moreover, certain authors have observed variations in shades ranging from brown or yellow and dark blue shades in bainitic microstructure.

3.5 Metallographic Studies

Metallography is fundamentally involving the examination and analysis of the structure and composition of metals by using metallurgical microscope and magnification in relation to its physical and mechanical properties and can be related to the microstructure. In

these studies, each of the samples was evaluated using an optical microscope (OM) to observe and identify the microstructure refinement in HAZ (Figure 3.13).

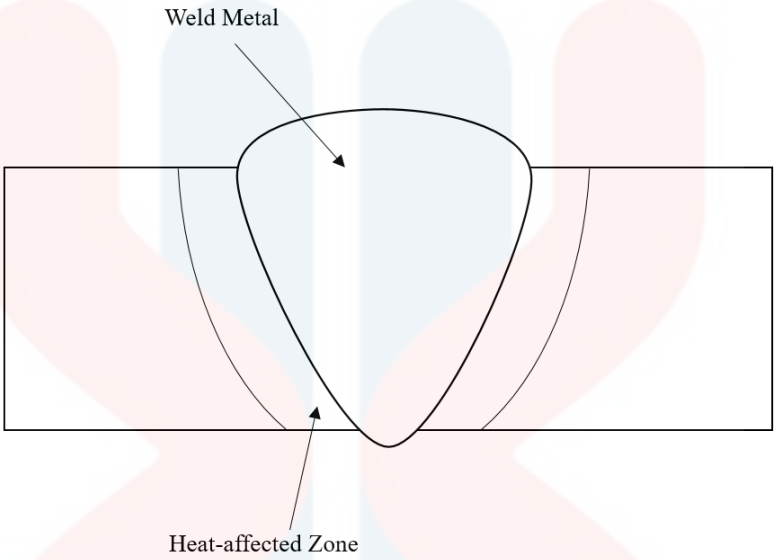

Figure 3. 13: Schematic diagram of weldment

Image analyser with metallurgical and microscope camera is depicted in figure 3.14 which enable accurate examination of microstructural features. Image analyser with metallurgical microscope and camera can be also referred as an optical microscope (OM). An optical microscope was used for microstructural investigation to show the microstructure of the weld and the heat-affected zone (HAZ) (Sharma & Shahi, 2014). Optical microscope that used offers a range of five magnification which are 5x, 10x, 20x, 50x and 100x. In this experiment, the microstructure of the welded specimen was observed under OM with different magnification (Ibrahim et al., 2012). In addition, this study performs microstructure analysis using nital etching and LePera etching techniques. Furthermore, the OM was employed to measure the bead geometry for the calculation of the dilution rate in this final year project. OM will reveal the details of weld bead and base metal providing comprehensive insights for the measurement of dilution rate.

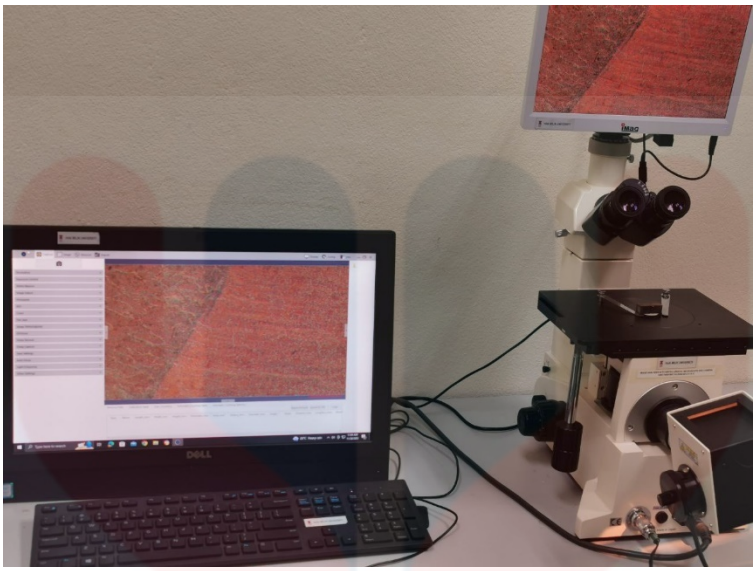

Figure 3. 14: Image analyser with metallurgical microscope and camera

3.6 Evaluation of Mechanical Properties

In this section, each sample was subjected to evaluation of mechanical properties such as hardness and toughness by following the ASTM standard and proper used of testing machinery.

3.6.1 Impact Toughness

Impact strength is the energy needed to fracture a notched specimen and is usually determined the Charpy V-notch impact test. Fracture toughness refers to the ability of a metal to withstand the crack propagation under the sudden application of significant force, once a crack has already formed. According to Sharma and Shahi (2014), the sample for the Charpy V-notch impact test was based on the ASTM: E23-12C Standard Test Methods for Notched Bar Impact Testing of Metallic Materials.

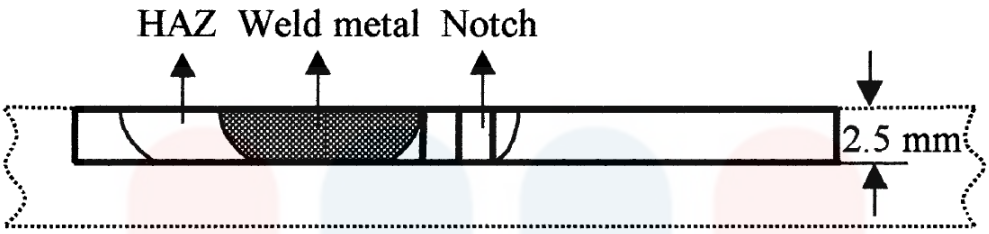

Figure 3. 15: Charpy impact test specimen for the toughness of HAZ

(Source: Eroglu et al., 1999)

According to Eroglu et al. (1999), the specimen dimensions for the Charpy impact test were 55 mm x 10 mm x 2.5 mm and based on Figure 3.15 the notch refers to where the HAZ toughness obtain. Samples were prepared at V and U groove with butt joint weld. Thus, the impact is directed towards the weld surface and V-notch was located at the opposite side of the weld surface. According to Pathak et al. (2020), weld metal exhibited higher hardness compared to HAZ and base metal. Welded samples were tested at three different temperatures which are room temperature (20°C), 0°C and -20°C to determine their impact resistance and behaviour in different conditions.

For testing at 0°C, samples were pre-cooled in the freezer a day prior. On the testing day, samples were removed from the chiller and soaked in an ice bath. Samples were selectively taken out as needed during the test to ensure accurate and controlled temperature. According to Wang et al. (2021), the temperature of liquid nitrogen (LN) is at -196°C. Hence LN was used as a cooling medium for samples tested at -20°C. Samples were pre-cooled directly in liquid nitrogen. The time between removing a sample from the cooling bath and actual impact for all recorded data was less than 5 seconds (Wang et al., 2021).

3.6.2 Hardness

Hardness can be defined as the ability of a material to resist indentation or penetration. According to Sharma and Shahi (2014) studied that the sample of the Vickers microhardness

test was based on the standard which is ASTM: E-384-11E1 Standard Test Method for Microindentation Hardness of Materials where the dimension in 50 mm x 5 mm x 3 mm (Ekaputra et al., 2018). In addition, the hardness of the sample is related to the depth of the indentation, the smaller indentation depth has higher hardness of the sample compared to larger indentation depth (Moore & Booth, 2015). The desired sample size was suitable for the microhardness test (Figure 3.16). According to Ekaputra et al. (2018), hardness measurements were conducted at intervals of 500 μm (Figure 3.17) across the base metal, heat affected zone and weld metal. Hardness tests were conducted in Advanced Technology Training Center (ADTEC) Kemaman at Terengganu using Vickers Hardness Tester. The hardness test was conducted using a diamond cone indenter with a load of 1 kgf as the applied force, and the measurements were taken at 10x magnification.

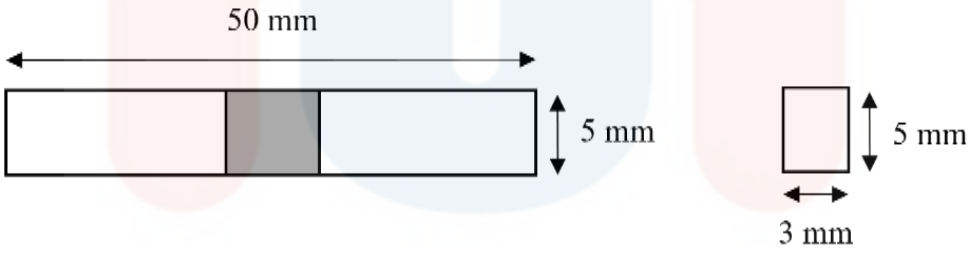

Figure 3. 16: ASTM: E-384-11E1 Microhardness sample preparation

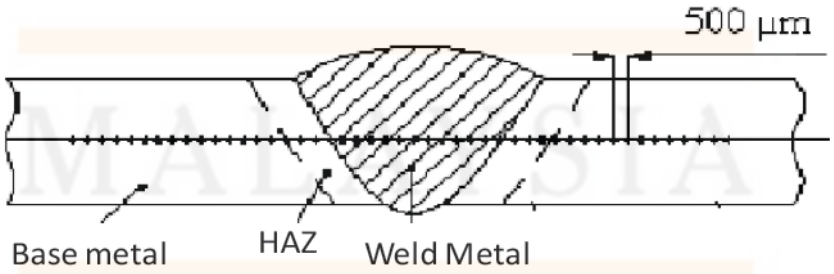

Figure 3. 17: The Vickers microhardness measurement

(Source: Ekaputra et al., 2018)

CHAPTER 4

RESULTS AND DISCUSSION

4.1 Visual Inspection of Weld Profile

Visual inspection is a non-destructive testing (NDT) weld quality check process which observed and analyse the weld profile of welded sample. In this section, the effect of groove shape specifically in single layer and multi-layer welding for V and U grooves was reviewed and analysed concerning the weld bead profile. Table 4.1 shows the welded samples with single and multi-layer welding for V and U grooves.

Table 4. 1: Welded samples with single and multi-layer welding for V and U grooves

	V Groove	**U Groove**
Single Layer		

Multi-Layer		

Single layer welding involves only one capping pass whereas multi-layer welding includes three capping passes. In the context of single layer welding, a V groove was denoted as SV and a U groove was referred to as SU. Similarly, for multi-layer welding, a V groove was labelled as MV and a U groove was designated as MU.

For single layer welding both SV and SU showed that surface defects such as porosity, crack or spatter were not detected. However, undercut was observed in SV while underfill was observed in SU. Conversely, in multi-layer welding an overfill was observed for the V groove whereas the U groove exhibited overlap along with spatter on the surface of the base metal.

4.1.1 Effect of Groove Shape on Weld Bead Profile in Single Layer Welding

Figure 4.1 depicts the weld bead geometry parameters which use to observe the weld bead profile such as weld toe angle, reinforcement height, penetration depth and weld bead size.

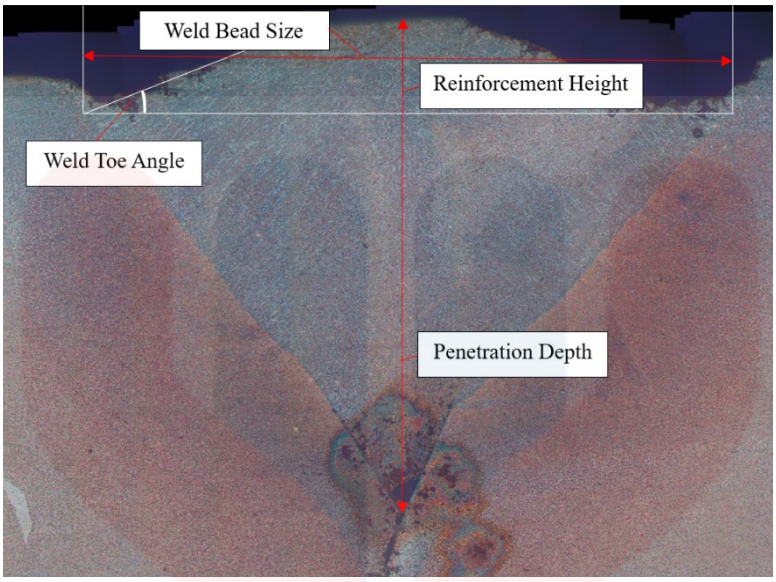

Figure 4. 1: Weld bead geometry parameters

The comparison between SV and SU weld configurations reveals distinct characteristics in terms of weld toe angle, reinforcement height, penetration depth, and weld bead size. In table 4.2, which outlines the weld profile of single layer welding for V (SV) and U (SU) grooves.

Table 4. 2: Weld profile of single layer welding for V and U grooves

	Weld Toe Angle (°)	**Reinforcement Height (mm)**	**Penetration Depth (mm)**	**Weld Bead Size (mm)**
SV	14.48	1.1	4.9	4.0
SU	23.31	1.3	3.2	0.7

SV demonstrates a moderate weld toe angle of 14.48°, accompanied by a 1.1 mm reinforcement height, a penetration depth of 4.9 mm, and a relatively larger weld bead size of 4.0 mm. In contrast, SU exhibits a steeper weld toe angle at 23.31°, a slightly higher reinforcement height of 1.3 mm, a lower penetration depth of 3.2 mm, and a smaller weld

bead size of 0.7 mm. These differences suggest that SV produces a weld with a broader and deeper profile, featuring a larger bead, while SU results in a steeper weld with a smaller bead size and less penetration depth. This can be justified due to the groove angle plays a crucial role in affecting the penetration depth during welding. V groove featuring an acute angle with a small angle exhibits deeper penetration due to the heat input only focus on a narrower space compared to the U groove which have a wider angle with wide opening. According to Pathak et al. (2020), groove angle significantly impacts the mechanical and structural properties of welded joints, revealing a decrease in reinforcement height as the groove angle increases from 40° to 75°.

4.1.2 Effect of Groove Shape on Weld Bead Profile in Multi-Layer Welding

In table 4.3, which outlines the weld profile of multi-layer welding for V (MV) and U (MU) grooves.

Table 4. 3: Weld profile of multi-layer welding for V and U grooves

	Weld Toe Angle (°)	**Reinforcement Height (mm)**	**Penetration Depth (mm)**	**Weld Bead Size (mm)**
MV	49.66	5.4	4.7	5.4
MU	31.75	2.3	6.7	7.3

Beginning with the weld toe angle, MV exhibits a steep angle of 49.66°, indicating an inclined and potentially penetrating weld, whereas MU features a comparatively milder weld toe angle of 31.75°, suggesting a less steep profile. Moving to the reinforcement height, MV showcases a substantial height of 5.4 mm, signifying a prominent buildup of material, while MU displays a lower reinforcement height of 2.3 mm. This can be justified due to groove v

has a narrower angle for molten metal into a more confined space while groove u with wider angle allows a broader weld pool during welding. Noting that multi-layer welding also known as multi pass welding which involves a layer-by-layer process. According to Pathak et al. (2020), measuring weld reinforcement height is crucial as it impacts the microstructure and mechanical behaviour of the welded joint. The penetration depth reveals another contrast, with MV presenting a moderate depth of 4.7 mm, and MU exhibiting a deeper penetration depth of 6.7 mm, suggesting a more profound weld penetration. Lastly, considering the weld bead size, MV and MU showcase bead sizes of 5.4 mm and 7.3 mm, respectively, portraying a larger bead size for MU. These differences underscore that MV tends to produce a steeper weld with substantial reinforcement, while MU results in a larger bead size and deeper penetration.

4.2 Grain size distribution of Heat Affected Zone

Grain size distribution is the arrangement and variation in sizes of individual grains within the microstructure of a sample. Based on figure 4.2, an analysis of grain size distribution using ImageJ was presented.

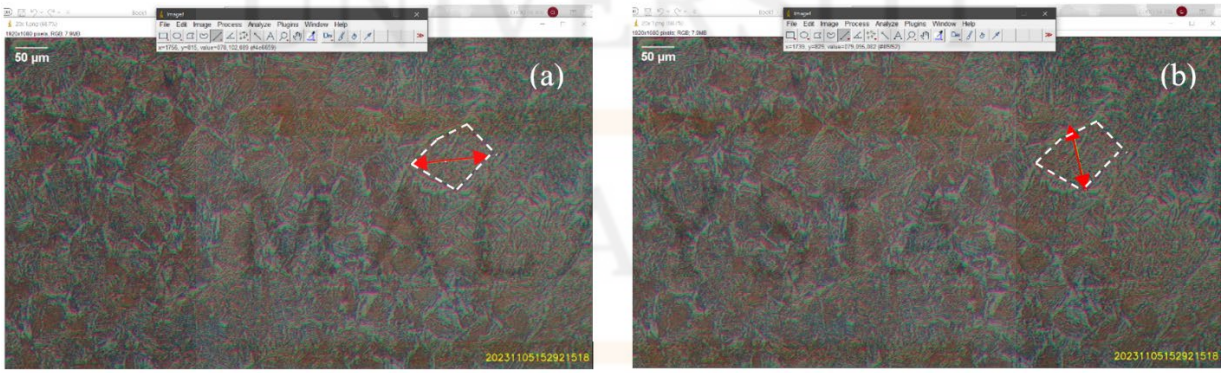

Figure 4. 2: Analyse grain size distribution using ImageJ

This analytical approach extends to specific zones such as coarse-grained heat affected zone (CGHAZ) and fine-grained heat affected zone (FGHAZ). In this section, the

average grain size for each zone was determined by collecting data on three individual grains from the respective zone.

4.2.1 Grain Size Comparison in Heat-Affected Zone for Single Layer Welding with V and U Grooves

Table 4.4 reveals a comparison of average grain sizes in the coarse-grained heat affected zone (CGHAZ) and fine-grained heat-affected zone (FGHAZ) for SV and SU.

Table 4. 4: Comparison of average grain size in CGHAZ and FGHAZ for SV and SU

	SV	**SU**
Average Grain Size of CGHAZ (µm)	92.81	107.50
Average Grain Size of FGHAZ (µm)	63.51	87.86

In CGHAZ, SU exhibits a larger average grain size of 107.50µm compared to SV with average grain size of 92.81µm. Similarly, in FGHAZ, SU results in a significantly larger average grain size of 87.86µm compared to SV with 63.51µm. Due to distinct heat dissipation characteristics in selected groove designs, there is a noticeable influence on the size and morphology of the microstructure, particularly in the CGHAZ and FGHAZ size. This variation in heat dissipation can affect grain size distribution, potentially impacting material properties.

4.2.2 Grain Size Comparison in Heat-Affected Zone for Multi-Layer Welding with V and U Grooves

Table 4.5 presents a comparative analysis of the average grain sizes in the Coarse-Grained Heat-Affected Zone (CGHAZ) and Fine-Grained Heat-Affected Zone (FGHAZ) for MV and MU.

Table 4. 5: Comparison of average grain size in CGHAZ and FGHAZ for MV and MU

	MV	**MU**
Average Grain Size of CGHAZ (µm)	92.30	92.15
Average Grain Size of FGHAZ (µm)	59.65	57.08

In the CGHAZ, MV exhibits a larger average grain size of 92.30µm compared to MU with average grain size of 92.15µm. Similarly, in the FGHAZ, MV results in a larger average grain size of 59.65µm compared to MU with average grain size of 57.08µm.

4.3 Microstructure Analysis with Nital Etching

In this section, microstructure analysis using nital etching was reviewed. Table 4.6 shows the samples after being etched based on V and U groove configurations in both single and multi-layer welds. The etching process involved the use of 2% nital solution to reveal the microstructure of the base metal, weld metal and heat affected zone.

Table 4. 6: Sample after nital etching

	V Groove	**U Groove**

Single Layer	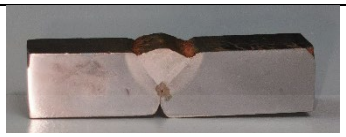	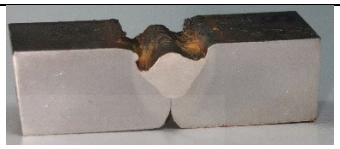
Multi-Layer		

4.3.1 Nital Etching Analysis of Single Layer V and U Groove Welds

The microstructures examination for single layer welds of V and U groove after nital etching were captured with an optical microscope with 10x magnification to measure the details of microstructural featured and phases present as shown in figure 4.3 and figure 4.4 respectively.

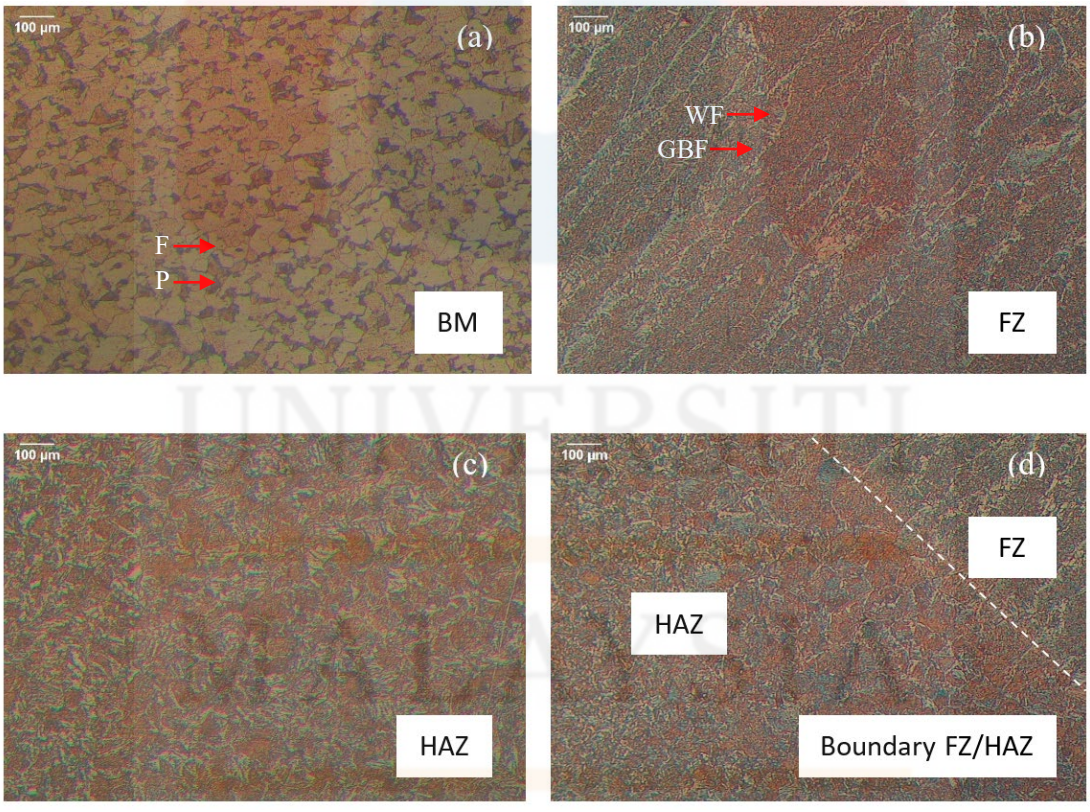

Figure 4. 3: Microstructures of single layer v-groove (a) BM (base metal); (b) FZ (fusion zone); (c) HAZ (heat affected zone) and (d) boundary between FZ and HAZ

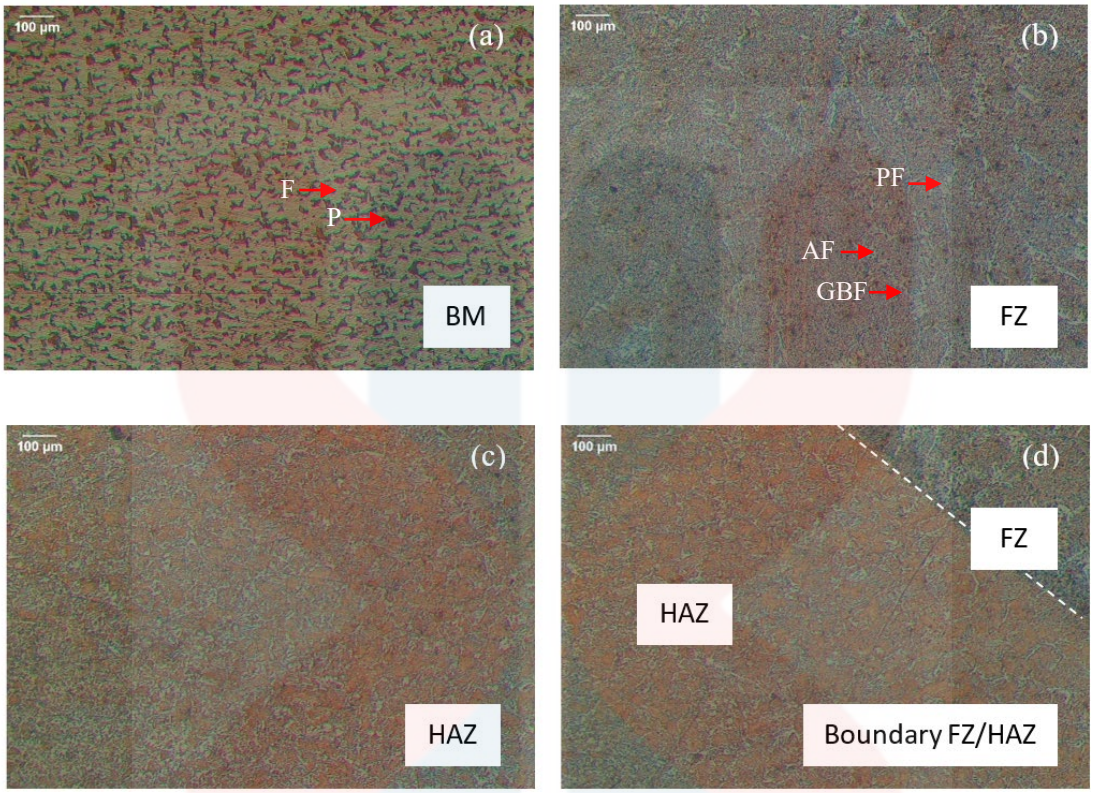

Figure 4. 4: Microstructures of single layer u-groove (a) BM (base metal); (b) FZ (fusion zone); (c) HAZ (heat affected zone) and (d) boundary between FZ and HAZ

The microstructure of the BM from figure 4.3 (a) and figure 4.4 (a) both reveal microstructure of ferrite (F) and pearlite (P). According to Ikram & Chung (2017), the microstructure of the BM exhibited a laminated structure with a distribution of ferrite and pearlite. Researchers further noted that ferrite appeared as the light regions while pearlite was observed in dark regions. The structure of the base metal in low carbon steel comprised approximately 80-85% ferrite and 15-20% pearlite (Bodude & Momohjimoh, 2015).

From Figure 4.3 (b), the columnar weld metal zone also known as fusion zone has a dendritic structure and reveal the presence of grain boundaries ferrite (GBF) and widmanstätten ferrite (WF). In contrast, figure 4.4 (b) displays a microstructure with GBF, acicular ferrite (AF) and polygonal ferrite (PF). Acicular ferrite was recognized for enhancing stell properties especially its toughness. Acicular ferrite is a microstructure composed of

small, interweaving ferrite plates formed within austenite grains during the cooling process. This microstructure enhances the material's mechanical properties, providing a balance of strength and toughness of the material (Sharma & Shahi, 2014). Grain boundaries ferrite offered a little resistance to cleavage crack propagation while widmanstätten ferrite is undesirable in welds due to its poor toughness might increases brittleness (Eroglu et al., 1999). According to the research done by Sharma & Shahi (2014), the micrographs of the weld metal zone in different joints reveal the presence of various morphological forms of ferrite, including acicular ferrite (AF), ferrite with a secondary phase (FS) or widmanstätten ferrite (WF) and allotriomorphic ferrite (ALF) or grain boundary ferrite (GBF).

Next, figure 4.3 (c) and figure 4.4 (c) depict the microstructure of the HAZ, highlighting the grain morphology in HAZ was different from BM. The microstructure of the HAZ showed large and coarse grains. In figure 4.3 (d) and figure 4.4 (d) shows the boundary between FZ and HAZ. The microstructure of HAZ showed significant large grains with variations in grain size across different zones such as coarse-grained HAZ (CGHAZ) and fine-grained HAZ (FGHAZ). Additionally, figure 4.5 and figure 4.6 shows a more detailed view of the microstructure in both the FZ and HAZ at 50x magnification in single layer welding of V and U and groove configurations.

Figure 4. 5: Microstructure of single v groove in HAZ under 50x magnification

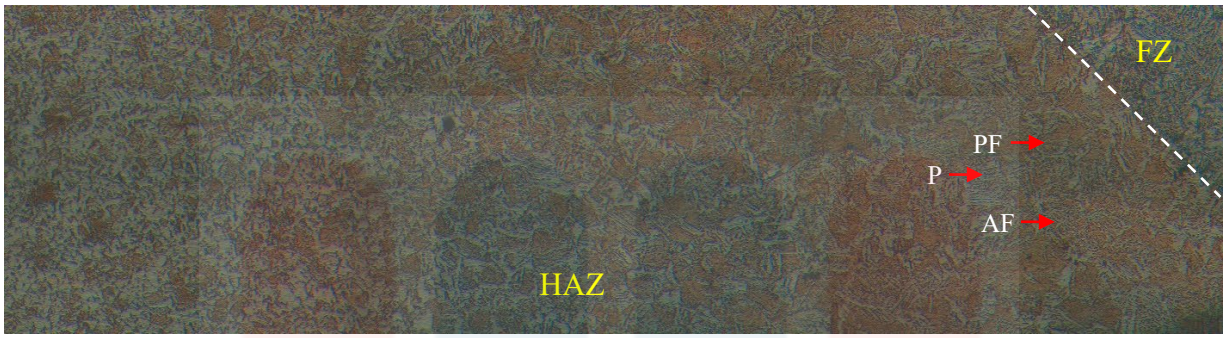

Figure 4. 6: Microstructure of single u groove in HAZ under 50x magnification

Based on the results of microstructure in single layer welding of V and U groove shows that the microstructure which direct contact with the fusion zone was large. Different regions within the HAZ experience varied levels of welding heat. The heat dissipates from the joint and heat transfer through the HAZ and indirect impact to the microstructure of each zone. According to Sharma & Shahi (2014), CGHAZ is adjacent to the fusion line and it undergoes austenitic transformation at high temperatures. The phase changes signify either the grain growth or recrystallization. According to the previous research done by Eroglu et al. (1999), polygonal ferrite (PF) and martensite (M) were only observed in CGHAZ.

From figure 4.5 the microstructure in CGHAZ with V groove welding consists of acicular ferrite (AF), grain boundary ferrite (GBF), ferrite with aligned secondary phase (FS (A)), pearlite (P) and upper bainite. On the other hand, based on figure 4.6 the microstructure in CGHAZ with U groove welding only consists of acicular ferrite (AF), polygonal ferrite (PF) and pearlite (P). The formation of these microstructure is due to when cooling down from the high temperature austenite phase, the carbon rich austenite undergoes transformation into different microstructures based on its carbon content. High carbon content leads to the formation of martensite, bainite or pearlite. On the other hand, low carbon content results in the production of polygonal ferrite (Zhao et al., 2019). The identification of martensite through nital etching is considered a preliminary assessment and a more precise analysis would necessitate detailed examinations using LePera etching.

Pearlite was identified in the microstructure of the HAZ of low carbon steel in both V and U groove welds along with various ferrite including acicular and grain boundary ferrite. Previous research by Khamari et al. (2020), justify that certain ferrite morphologies such as acicular, polygonal and grain boundary ferrite exhibit lower hardness values and do not contribute to increase hardness in that region. Pearlite appears as lamellar layered structures which consist of alternating layers of ferrite and cementite. According to Mansjur et al. (2019), the grain structure of pearlite in the HAZ exhibit coarser grain compared to base metal. In addition, in CGHAZ both single layer welding V and U groove welds exhibit the presence of acicular ferrite (AF). Its formation in a fine needle structure which enhance the material's toughness and resistance to brittle fracture.

The formation of upper bainite in SV is due to the heat treatment during the welding process. Bainite is a phase transformation consists of ferrite and cementite. This microstructure can be differentiated into two main types which are upper bainite and lower bainite. Distinction of these two bainite is based on the transformation temperature and microstructural features. The presence of upper bainite in the CGHAZ of SV is likely a result of the high temperatures experienced by the CGHAZ near the fusion zone during welding. The presence of upper bainite in SV is characterized by a microstructure consisting of a fine, acicular (needle-like) ferrite structure embedded in a matrix of cementite (Xiao et al., 2020). In addition, ferrite with aligned secondary phase in SV suggest that this alignment might influences the mechanical properties of materials.

4.3.2 Nital Etching Analysis of Multi-Layer V and U Groove Welds

The microstructures examination for multi-layer welds of V and U groove after nital etching were captured with an optical microscope with 10x magnification to measure the

details of microstructural featured and phases present as shown in figure 4.7 and figure 4.8 respectively.

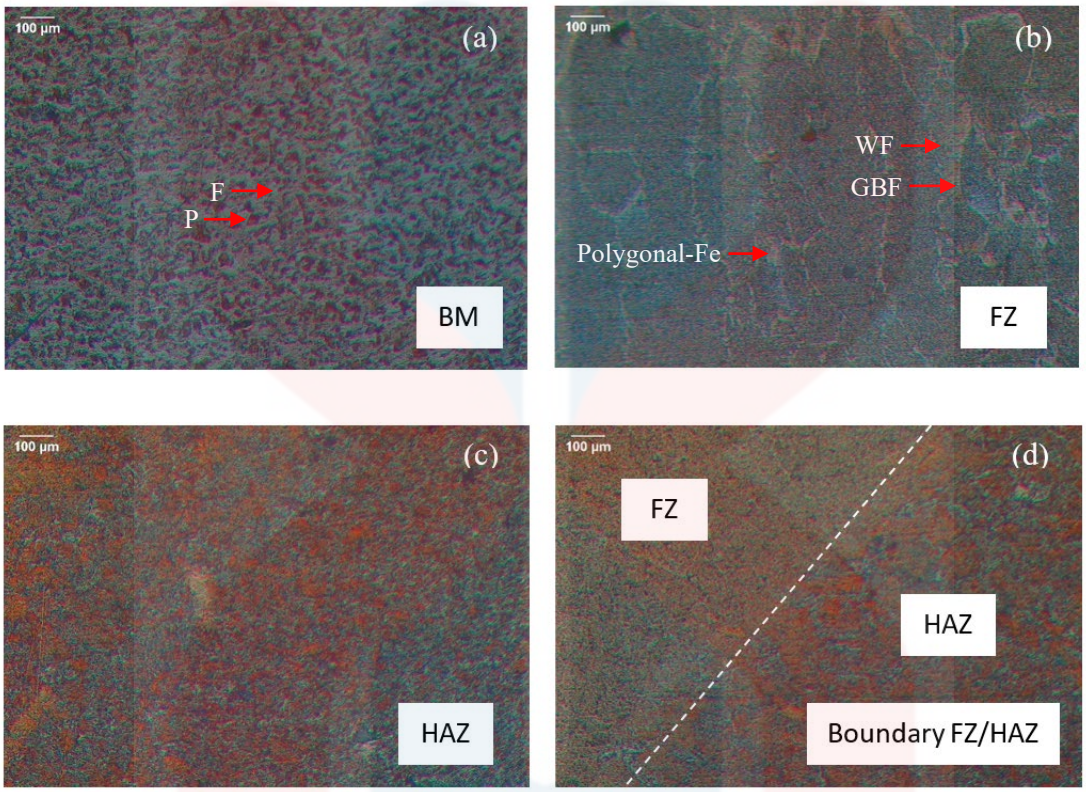

Figure 4. 7: Microstructures of multi-layer v-groove (a) BM (base metal); (b) FZ (fusion zone); (c) HAZ (heat affected zone) and (d) boundary between FZ and HAZ

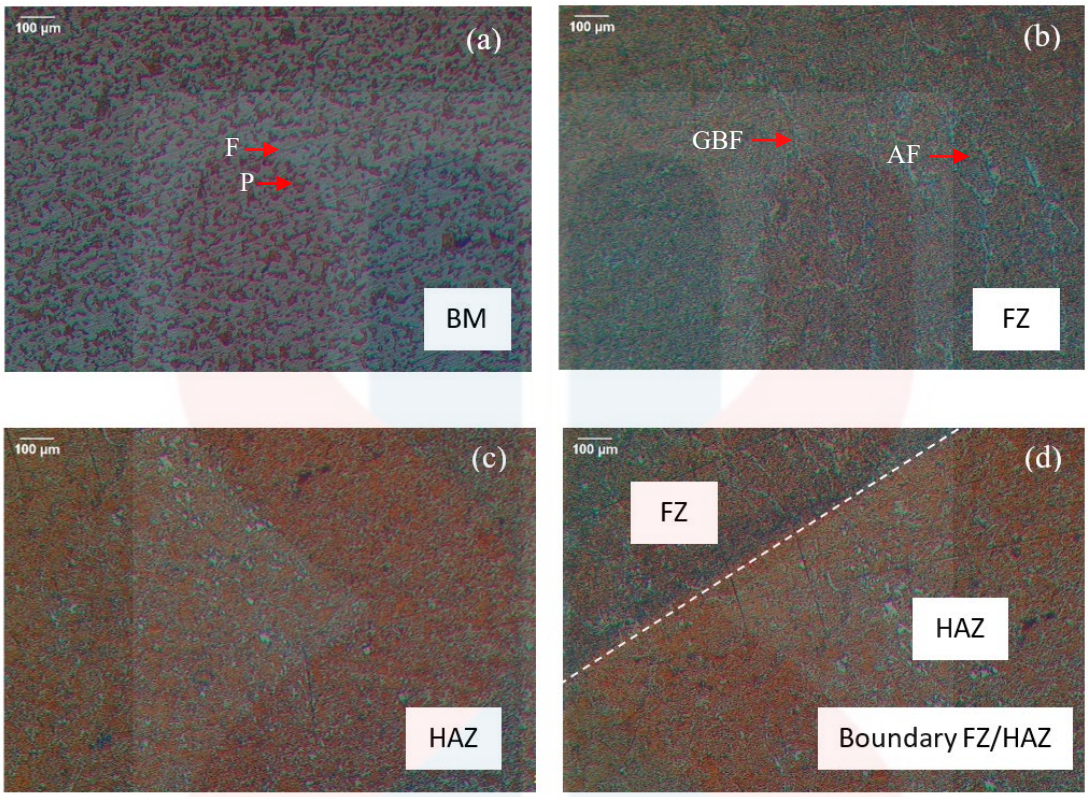

Figure 4. 8: Microstructures of multi-layer u-groove (a) BM (base metal); (b) FZ (fusion zone); (c) HAZ (heat affected zone) and (d) boundary between FZ and HAZ

The microstructure of the BM from figure 4.7 (a) and figure 4.8 (a) both reveal microstructure of ferrite (F) and pearlite (P). Followed by the microstructure of fusion zone was depicted in figure 4.7 (b) and figure 4.8 (b). In the fusion zone of multi-layer V groove welding, the microstructure reveals the presence of widmanstätten ferrite (WF), grain boundary ferrite (GBF) and polygonal ferrite (PF) while u groove displays GBF and acicular ferrite (AF). However, weld sample MV reveal the presence of widmanstätten ferrite (WF) which was not observed in MU. According to (Dissertation et al., 2021), widmanstätten ferrite exhibit a side plate morphology and grows within the austenite grain during the process. Additionally, figure 4.9 and figure 4.10 shows a more detailed view of the microstructure in both the FZ and HAZ at 50x magnification in single layer welding of V and U and groove configurations.

Figure 4. 9: Microstructure of multi v groove in HAZ under 50x magnification

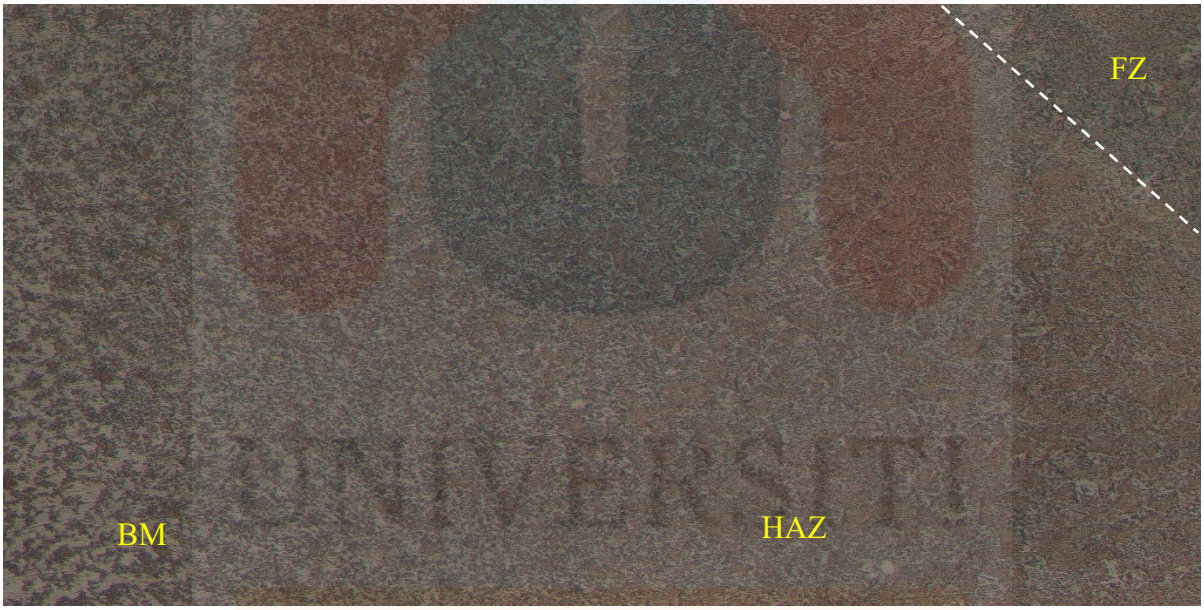

Figure 4. 10: Microstructure of multi u groove in HAZ under 50x magnification

In multi-layer welding, the process involves stacking up multiple passes of filler material, contributing to the formation of a layered and reinforced weld structure. The observation that the formed grain-refining sizes in multi-layer welding were much finer compared to single layer welding. From the results, a closer examination reveals notable recrystallization phenomena occurring within the HAZ. In this region, it undergoes effective

heat treatment due to the temperature exceeding the critical point to fully transform from austenite. At this elevated temperature, austenite phase can transform into various structural phases such as martensite, bainite, pearlite or ferrite under suitable cooling rate.

The microstructure observed in multi-layer welding of V and U groove reveals the same microstructural compared with single layer welding but with smaller grain size. Crystalline regions form due to temperature variations during different welding pass. In the second welding layer, HAZ from the first layer undergoes another heating and cooling cycle. The second heating period has a lower temperature compared to the first layer. Thus, the formation of fine grain austenite was resulted. The slower cooling rate, attributed to the preheated welding plate and contributes to smaller grain size.

4.4 Microstructure Analysis with LePera Etching

According to Ko et al. (2022), nital etching generally used to categorize the microstructure such as pearlite and martensite which reveal in black and ferrite in white. However, to accurately distinguish phases that is difficult to identified, LePera etching is employed. LePera etching able to provide distinct phase analysis such as brown for bainite, white for martensite and blue or green is ferrite.

In this section, microstructure analysis using LePera etching was reviewed. Table 4.7 shows the samples after being etched based on V and U groove configurations in both single and multi-layer welds. The etching process involved the use of LePera solution, mixture of two reagents which are sodium metabisulfite ($Na_2S_2O_5$) and picric acid [$(O_2N)_3C_6H_2OH$] to reveal the microstructure of the heat affected zone.

Table 4. 7: Samples after LePera etching

	V Groove	U Groove
Single Layer	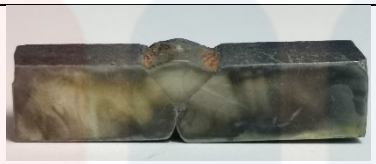	
Multi-Layer		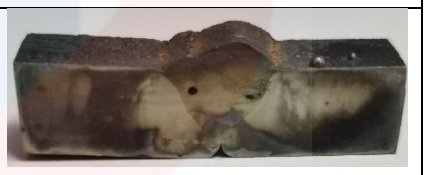

4.4.1 LePera Etching Analysis of Single Layer V and U Groove Welds

Furthermore, the microstructures examination of heat affected zone (HAZ) for single layer welds of V and U groove after LePera etching were captured with an optical microscope with 50x magnification to measure the details of microstructural featured and phases present as shown in figure 4.11 and figure 4.12 respectively.

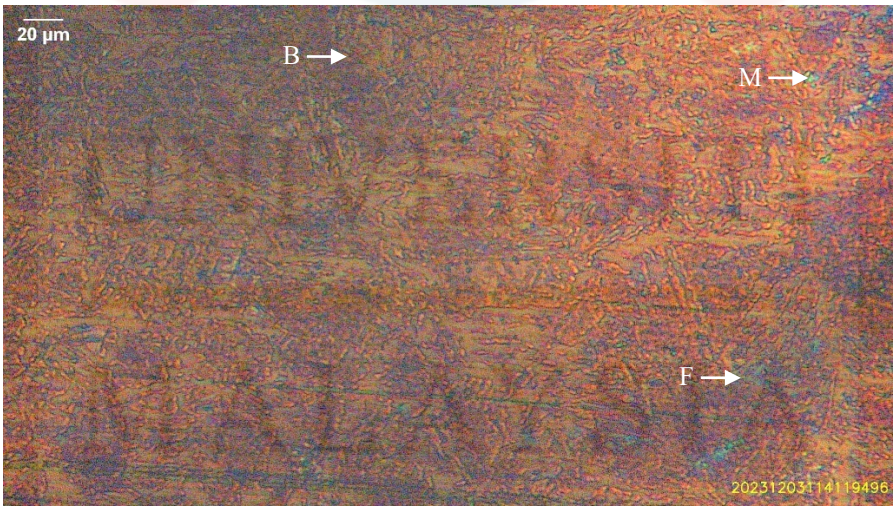

Figure 4. 11: HAZ microstructure for single layer weld with V-groove

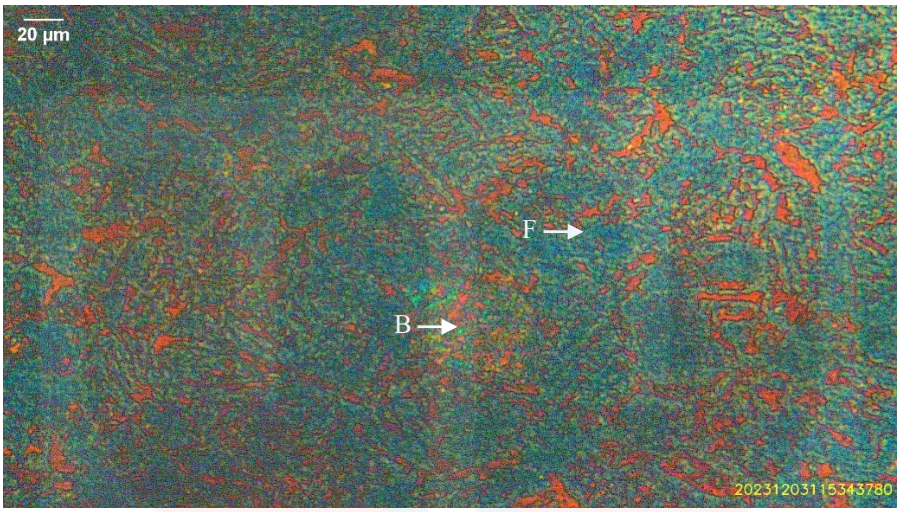

Figure 4. 12: HAZ microstructure for single layer weld with U groove

In the Heat-Affected Zone (HAZ) analysis of low carbon steel using LePera etching, single-layer welding with a V-groove reveals the presence of bainite, ferrite, and martensite. Conversely, U groove welding in the HAZ displays bainite and ferrite. The distinctive microstructures and properties observed through LePera etching highlight that, in V-groove welding, the inclusion of martensite contributes to enhanced strength, while U groove welding, characterized by bainite and ferrite, emphasizes a balance of strength and ductility in the HAZ. According to Ko et al. (2022), ferrite phase reveal in yellow/blue colour while bainite phase reveal in a blue-brown colour. Acicular (needle-like) structure of bainite which consists of fine ferrite plates or laths embedded in a matrix of carbon-enriched austenite was observed in single and multi-layer welding with V and U groove (figure 4.11 to figure 4.14).

4.4.2 LePera Etching Analysis of Multi-Layer V and U Groove Welds

The microstructures examination of heat affected zone (HAZ) for multi-layer welds of V and U groove after LePera etching were captured with an optical microscope with 50x magnification to measure the details of microstructural featured and phases present as shown in figure 4.13 and figure 4.14 respectively.

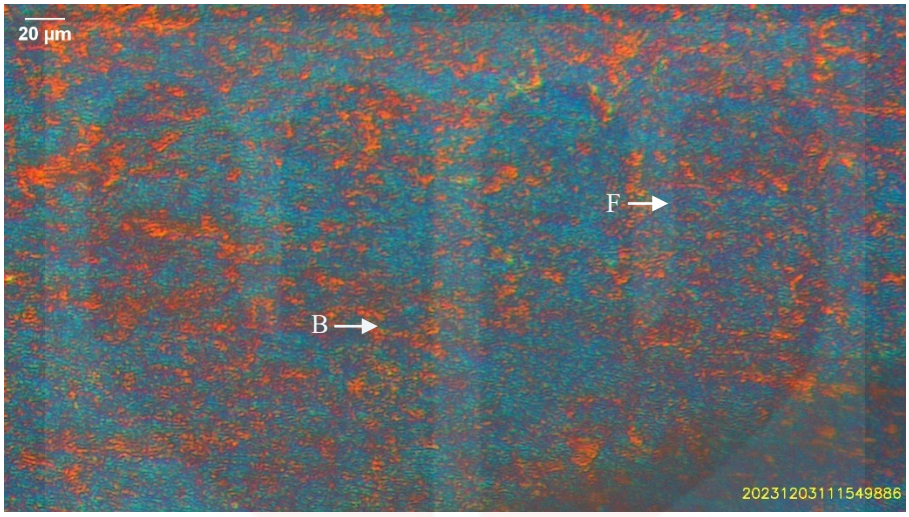

Figure 4. 13: HAZ microstructure for multi-layer weld with V-groove

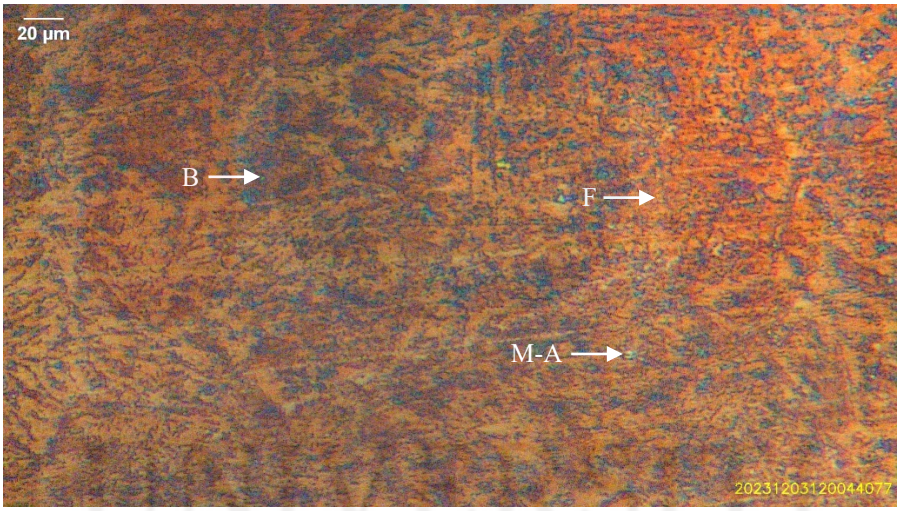

Figure 4. 14: HAZ microstructure for multi-layer weld with U groove

Nital etching is widely employed in the microstructure observation of HAZ especially CGHAZ, however it is less effective due to the small size of Martensite-Austenite constituent (M-A). According to Mendonça et al. (2020), LePera etching highlights martensite reveal in bright white with retained austenite as an MA constituent, while ferrite appears in a light brown and bainite in a dark brown tone. The appearance of M-A constituents is due to the rapid cooling conditions experienced during welding. During the welding process, the material undergoes a rapid transition from high temperatures to lower temperatures as the

welding arc is applied and removed. This abrupt cooling leads to variations in the microstructure, especially in the HAZ. The cooling rate influences the kinetics of phase transformations, and the quick cooling associated with welding can result in the formation of complex microstructures, including M-A constituents (Mao et al., 2019).

4.5 Dilution Rate in Dissimilar Groove Shape

Based on figure 4.15, dilution rate for single layer welding with dissimilar groove shape was studied.

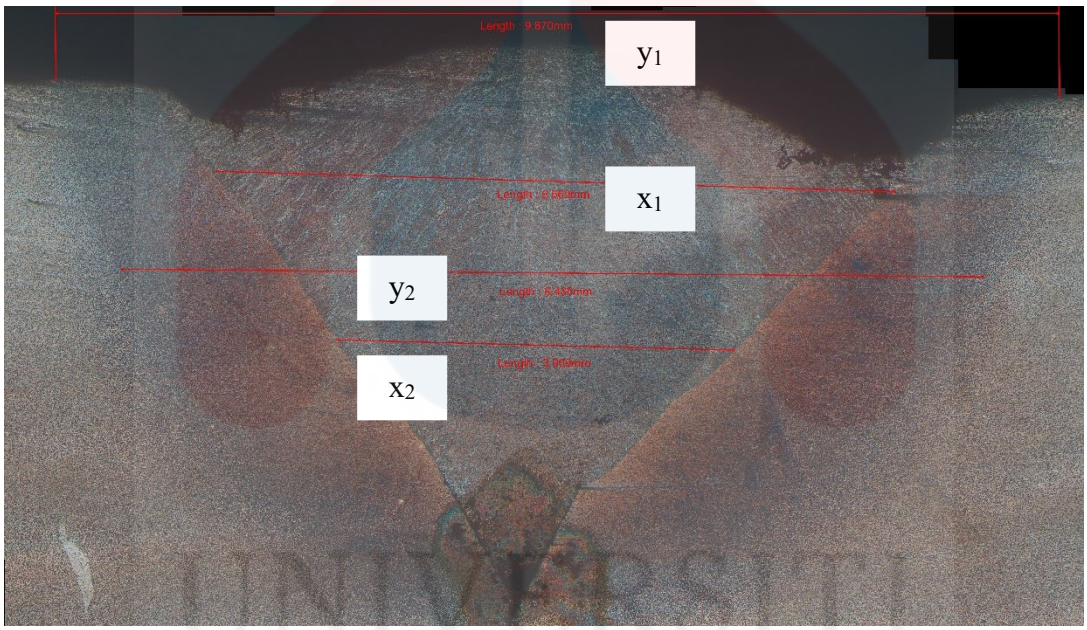

Figure 4. 15: Measurement for dilution rate for single layer welding

According to Valdenebro et al. (2022), dilution refers to the mixture of the base metal with the molten filler metal. Dilution rate was determined by the ratio of these two components. Average dilution rates for single layer welding of V and U groove were calculated using the formula shown.

$$Dilution\ Rate\ 1 = \frac{y_1 - x_1}{y_1 + x_1} \times 100\%$$

$$Dilution\ Rate\ 2 = \frac{y_2 - x_2}{y_2 + x_2} \times 100\%$$

$$Average\ of\ Dilution\ Rate\ (\%) = \frac{Dil.R_1 + Dil.R_2}{2}$$

Table 4.8 has shown that the average dilution rate for single layer welding under consistent in heat input but different groove shape.

Table 4. 8: Average dilution rate for single layer welding

Dilution Rate (%) / **Grooves**	**SV**	**SU**
Dilution Rate 1	19.35	14.85
Dilution Rate 2	36.94	35.18
Average Dilution Rate	**28.15**	**25.02**

Previous research done by Ebrahimi et al. (2021) on the effect of groove shape on molten metal behaviour in GMAW has shown that the heat distributed to the solid material significantly influences the shape of the melt pool. Even the heat input applied is consistent, the shape of the melt pool was varied significantly with different groove shapes. Dilution rate 1 and dilution rate 2 were utilized to calculate the average dilution rate for groove V and U. The average dilution rates for grooves SV and SU are 28.15% and 25.02% respectively. The analysis emphasizes that the dilution rate for single layer welding of V-groove is higher compared to U groove, highlighting the influence of groove shape on the average dilution rate in single layer welding process. This can be justified by the design of the V-groove which has an acute angle of 70° which allows deep penetration. In contrast, the U groove with a 40° angle featured a wider opening and resulting a shallow penetration. Deeper penetration

required large amount of filler material to mix with the base metal whereas shallow penetration only allows small amount of filler material to mix with the base metal.

4.6 Mechanical Properties

Mechanical properties play a crucial role in welding, offering insights into the behaviour of the material. In this final year project, Charpy impact test and Vickers hardness test serves as fundamental tools to evaluate the toughness, resistance to fractures and overall durability.

4.6.1 Microhardness Studies

Microhardness studies provides a crucial insight into the mechanical properties of materials and it help to relate microstructure details to enhance understanding and quality controls of materials. Figure 4.16 introduces the Falcon 400 Vicker Hardness Tester, a cutting-edge tool specialized for precise hardness testing in welding applications.

Figure 4. 16: Falcon 400 Vicker Hardness Tester

Figure 4.17 presents a schematic diagram of microhardness measurement, highlighting the indentation process across sample at a total 11 points from left to right. Indentation within the HAZ includes CGHAZ, FGHAZ and ICHAZ which noted points was 2, 3, 4, 8, 9 and 10. Followed by the indentation in fusion zone that includes a centreline at point 5 to 7. The microhardness analysis involved applying a 1kg load in the transverse direction to the weld bead. This testing method provides insights into the hardness characteristics of the material at a microscale level.

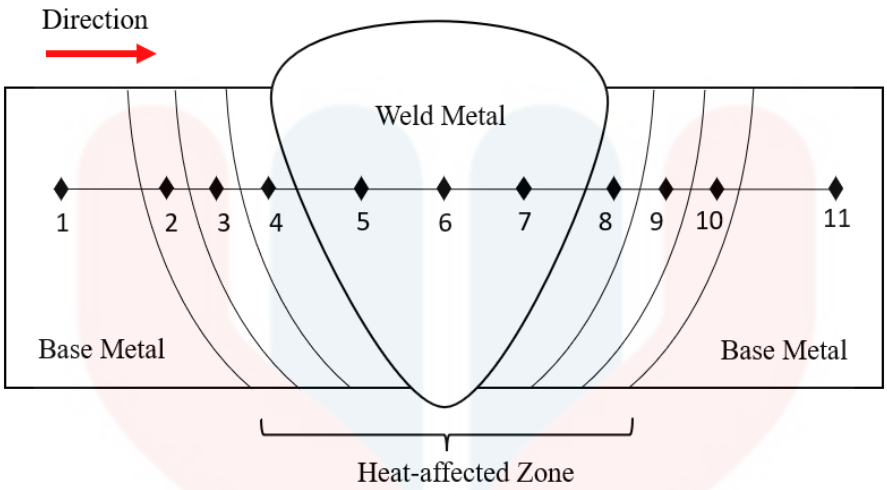

Figure 4. 17: Schematic diagram of microhardness measurement

Figure 4.18 depicts a Vicker hardness graph illustrating the comparative hardness values of single layer V and U groove welds which highlights differences in mechanical properties of both grooves.

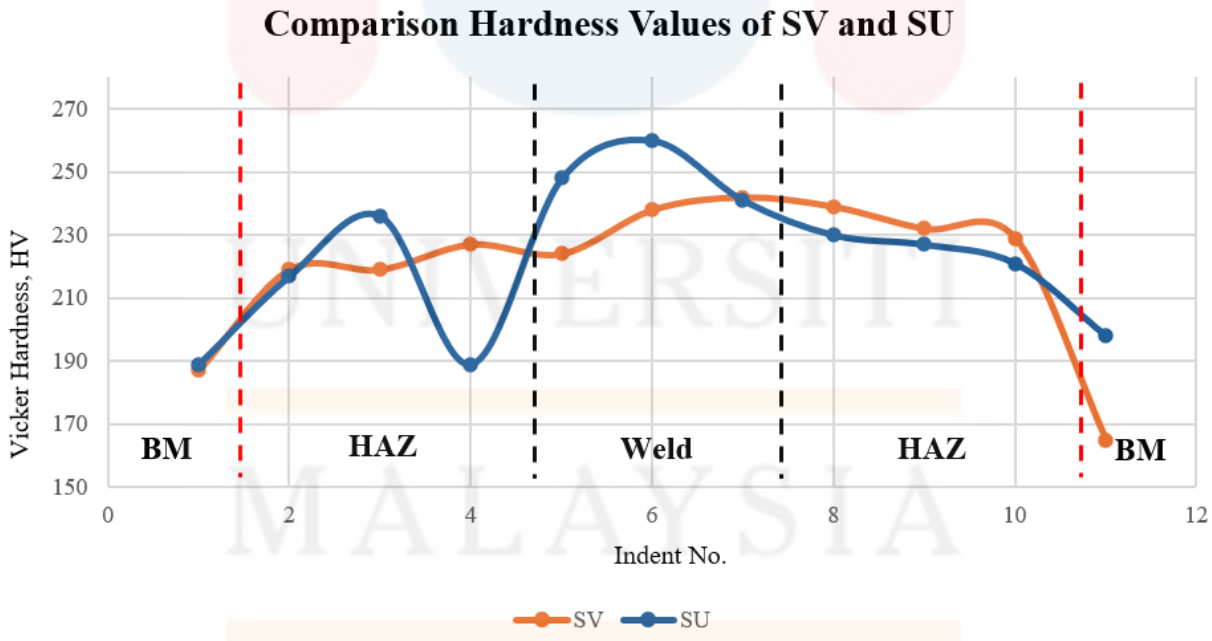

Figure 4. 18: Comparison Hardness Values of SV and SU

Based on the result, fusion zone (point 5 to 7) exhibits notably high hardness values for both V and U grooves single layer welding. The hardness value peak for SV occurs at point 7 with a value of 242 HV while for SU the peak is at the centreline of fusion zone with a value of 260 HV. The hardness values of SV and SU are transformed into a graph to visually depict and analyse the variations, enabling a more accessible interpretation of trends and patterns in their respective hardness profiles within the weld structure. Based on the graph, hardness values at the fusion zone (FZ) indicated SU have higher hardness than SV. This suggests that microstructure polygonal ferrite and acicular ferrite in fusion zone of SU provides a good toughness and ductility to the material. On the other hand, the appearance of widmanstätten ferrite (WF) in SV can adversely affect in mechanical properties such as toughness.

Followed by, Figure 4.19 depicts a Vicker hardness graph illustrating the comparative hardness values of multi-layer V and U groove welds which highlights differences in mechanical properties of both grooves.

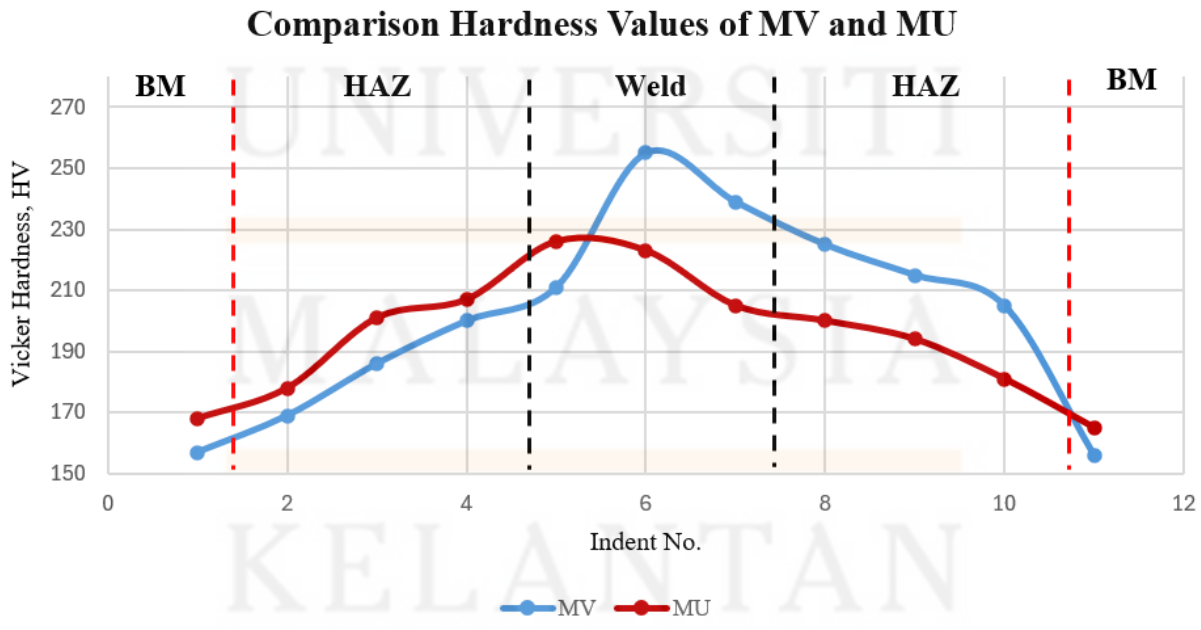

Figure 4. 19: Comparison Hardness Values of MV and MU

Based on the result, fusion zone (point 5 to 7) exhibits notably high hardness values for both V and U grooves multi-layer welding. The hardness value peak for MV occurs at the centreline of fusion zone with a value of 255 HV while for MU the peak is at point 5 with a value of 226 HV. The hardness values of MV and MU are transformed into a graph to visually depict and analyse the variations, enabling a more accessible interpretation of trends and patterns in their respective hardness profiles within the weld structure. Based on the graph, hardness values at the fusion zone (FZ) indicated MV have higher hardness than MU. This suggests that the observed difference in hardness values may be influenced by factors such as cooling rates, alloy composition, and heat treatment conditions, which result in distinct microstructural features (Ali et al., 2019).

4.6.2 Impact Properties

Based on figure 4.20 (a) impact strength evaluation was carried out using GT-7052-H50 Charpy impact tester with a capacity 50 kg.m, pendulum length of 850mm and 32.16 kg for horizontal weight of pendulum. The preparation of welded samples for both single and multi-layer welding with V and U groove were shown in figure 4.20 (b).

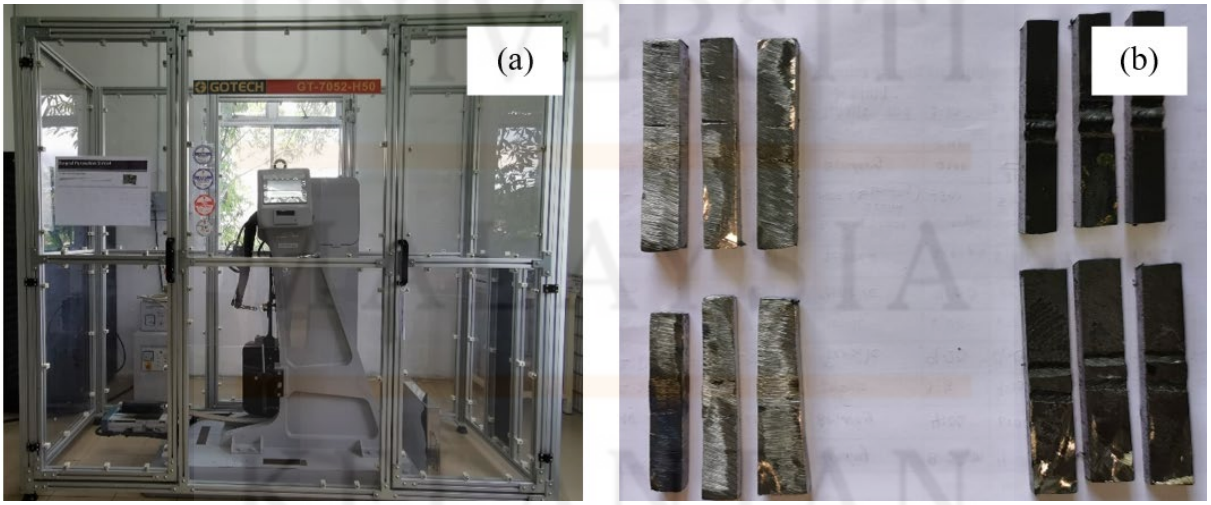

Figure 4. 20: Impact strength evaluation (a) GT-7052-H50 Charpy impact tester; (b) Welded sample for impact test

Charpy impact test is used to determine the resistance of samples to sudden impacts(Parmar et al., 2021). In other words, Charpy impact testing is a method used to measure the impact toughness of a material. The testing was conducted following the ASTM E23 standard test methods for notched bar impact testing of metallic materials. The welded samples were tested at three different temperatures which are room temperature (20°C), 0°C and -20°C to determine their impact resistance and energy absorbed in different conditions.

Table 4.9 presents the results of the impact test for single layer welding at different temperatures and groove design.

Table 4. 9: Samples after impact test for single layer welding

Temperature (°C) / **Grooves**	SV	SU
20°C	Brittle 	Ductile 
0°C	Brittle 	Brittle 
-20°C	Brittle 	Brittle 

According to Waqas et al. (2019), toughness is used to study the ability of absorb energy and determining the ductile or brittle behaviour. At room temperature (20°C), SV exhibit a brittle fracture while SU display a ductile fracture. However, at temperature of 0°C

and -20°C both SV and SU exhibited brittle fractures. The absorb energy by single layer V and U groove welds were recorded in table 4.10.

At room temperature (20°C), both SV and SU absorbed similar energy recording values of 16.12 J. However, at 0°C SV showed a slightly lower absorbance of energy at 15.96 J compared to SU with 16.54 J. At temperature -20°C, SV exhibit a higher absorbance at 16.78 J compared to SU with 16.77 J. Both SV and SU indicate the highest absorb energy when samples test under -20 °C. According to Wang et al. (2021), most metals tend to exhibit reduce in ductility and impact toughness at low temperature. This behaviour is often attributed to a decrease in atomic vibrations, causing the material to become more brittle. The reduction in temperature leads to a more ordered and rigid atomic structure, making it challenging for dislocations to move through the crystal lattice (Callister, 2019).

Table 4. 10: Absorbed energy at different temperatures for single layer V and U groove

Temperature (°C) / **Grooves**	SV	SU
	Absorb Energy (J)	
20°C	16.12	16.12
0°C	15.96	16.54
-20 °C	16.78	16.77

Based on figure 4.21, data collected were construct into Ductile-to-Brittle transition temperature curve (DBTT) to provide a comprehensive visualization of the absorbance of energy changes across three different temperatures for SV and SU.

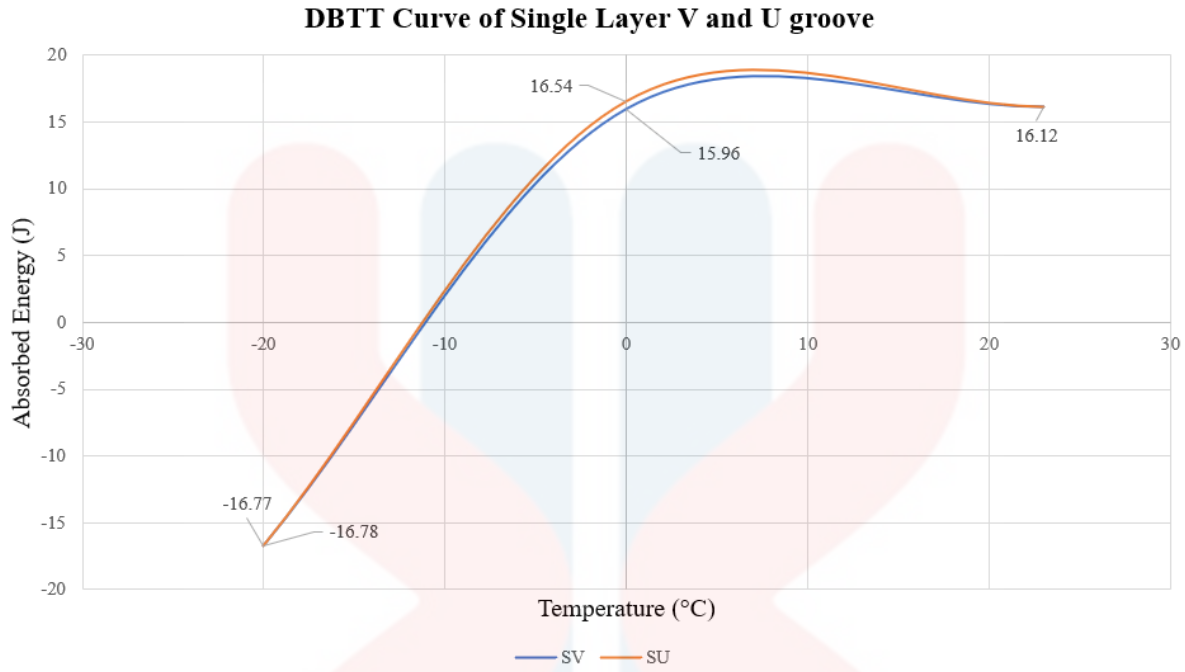

Figure 4. 21: Ductile-to-Brittle transition temperature curve of single layer V and U groove

The results shown that, at temperature 0°C the energy absorb by SV is slightly lower than SU. This indicates that SV shift towards a more brittle state when temperature is at 0°C. In addition, other than charpy impact test the fracture surface of the specimens was examined to offer a valuable insight. Table 4.11 shows the fractographs of single layer welding for V and U groove after impact test under different temperatures.

Table 4. 11: Fractographs of Charpy impact test of single layer welding for V and U groove

Temperature (°C) / **Grooves**	SV	SU
20°C		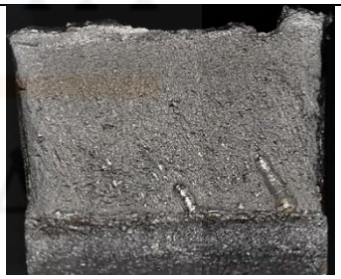

0°C		
-20°C		

According to Waqas et al. (2019), ductile fractures exhibit a dimpled surface resulting from material tearing and plastic deformation. On the other hand, brittle fractures are characterized by cleavage facets and minimal plastic deformation. Samples were prepared to evaluate the performance of the fracture analysis technique proposed in this final year project. Figure 4.22 depicts the technique used for the conversion of impact test fracture image using ImageJ.

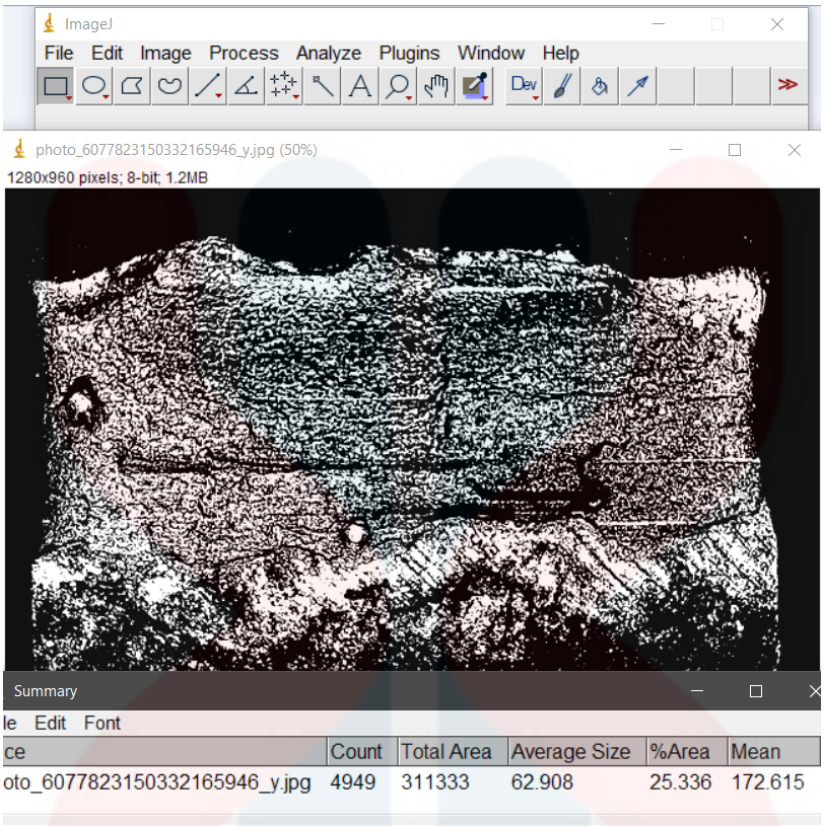

Figure 4. 22: Conversion of impact test fracture image using ImageJ

The fractographs of both single and multi-layer welding with V and U groove were converted into the grayscale image using ImageJ. A threshold image was generated by applying guided image filtering to the fracture image. White zone of the image represents ductile whereas the dark zone of the image represents brittle. Area percentage of ductile brittle regions was calculated and recorded. Table 4.12 shown the resultant images of ductile-brittle fracture areas of single layer welding of V and U groove under different temperatures.

Table 4. 12: Percentage calculation of ductile-brittle fracture areas in single layer welding at various temperatures with V and U grooves

Temperature (°C) / **Grooves**	SV	SU
	Area % of Ductile-Brittle Surface	

20°C	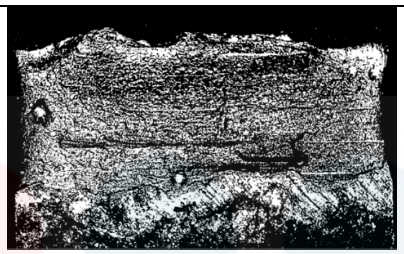 D= 25.34% B= 74.66%	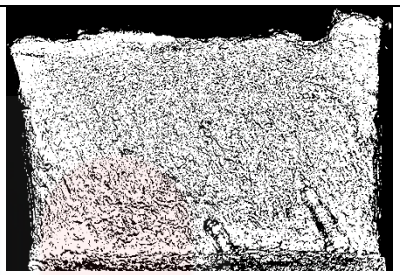 D= 61.27% B= 38.73%
0°C	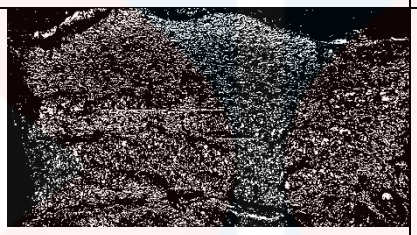 D= 21.34% B= 78.66%	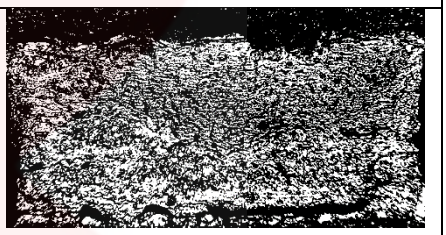 D= 35.27% B= 64.73%
-20°C	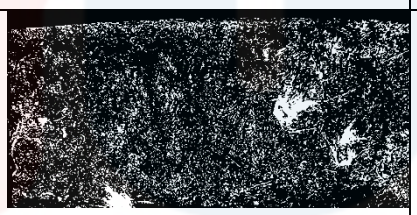 D= 20.05% B= 79.95%	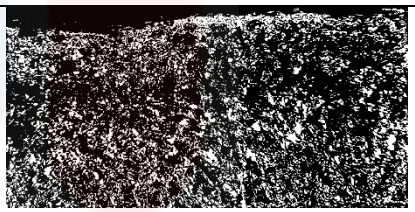 D= 24.47% B= 75.53%

At room temperature (20°C), the V-groove shows a higher percentage of brittle fracture area at 74.66% compared to the U groove with 38.73%. In contrast, U groove has a higher ductile fracture area at 61.27% while the V-groove has 25.34%. According to the previous research by M. Singh et al. (2020), the variation in weld groove volume has a significant impact on the joint's toughness. The smallest the groove volume will improve the impact toughness. This can be justified by the groove design in this final year project. The V groove has a groove angle of 70° whereas the U groove features a groove angle of 40°, resulting in the smallest groove volume.

Followed by testing conducted at 0°C, both V and U grooves exhibit brittle behaviour. SV has a slightly higher percentage of brittle surface area at 78.66% compared to SU where the brittle surface is 64.73%. According to Bonnekoh et al. (2019),analysis of the fracture surface exhibits brittle fracture behaviour in the test sample at low temperatures. Conversely, as the temperature rises, a shift towards ductile behaviour. Additionally, both SV and SU exhibit brittle behaviour when tested at -20°C with both exhibiting higher brittle surface areas compared to the testing conducted at 0°C.

Besides single layer welding, comprehensive tests have been carried out on multi-layer welding at three different temperatures to evaluate the corresponding toughness properties. Table 4.13 presents the results of the impact test for multi-layer welding at different temperatures and groove design.

Table 4. 13: Samples after impact test for multi-layer welding

Temperature (°C) / **Grooves**	MV	MU

20°C	Ductile 	Ductile 
0°C	Ductile 	Ductile 
-20°C	Brittle 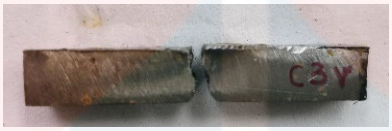	Brittle 

At room temperature (20°C) and 0°C both MV and MU exhibits ductile behaviour whereas sample tested at -20°C shows a brittle behaviour. The absorb energy by multi-layer V and U groove welds were recorded in table 4.14.

Table 4. 14: Absorbed energy at different temperatures for multi-layer V and U groove

Temperature (°C) / **Grooves**	MV	MU
	Absorb Energy (J)	
20°C	15.30	14.27
0°C	15.89	14.75
-20 °C	16.81	16.93

Samples tested at room temperature (20°C) and 0°C shows that MV exhibits higher absorbed energy compared with MU. On the other hand, at -20 °C impact test results show

that MU exhibits higher absorption energy compared with MV. In various applications, multi-layer welding produces a recrystallization effect which lead to affect the mechanical properties (Jorge et al., 2021). Based on figure 4.23, data collected were construct into Ductile-to-Brittle transition temperature curve (DBTT) to provide a comprehensive visualization of the absorbance of energy changes across three different temperatures for MV and MU.

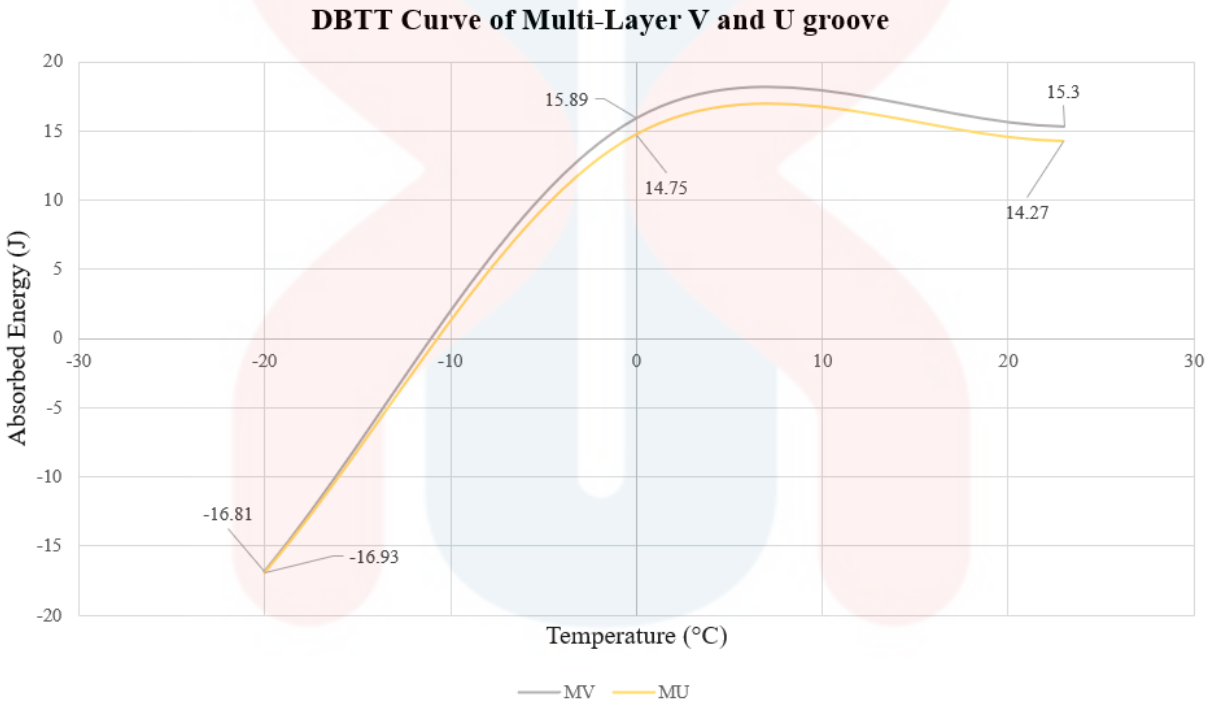

Figure 4. 23: Ductile-Brittle transition temperature curve of multi-layer V and U groove

From the results it shown that as the temperature decrease, the absorb energy increase thus improve impact toughness. Fractographs of multi-layer welding for V and U groove after impact test under different temperatures are shown in table 4.15. Further examination of the ductile-brittle surface area is illustrated in table 4.16, utilizing ImageJ for image analysis.

Table 4. 15: Fractographs of Charpy impact test of multi-layer welding for V and U groove

Temperature (°C) / **Grooves**	MV	MU
Room Temperature		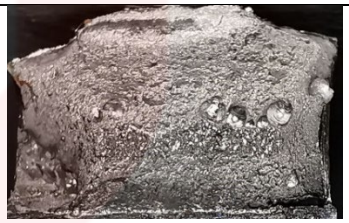
0°C	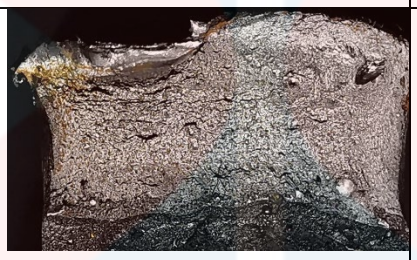	
-20°C	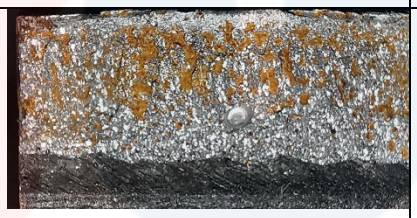	

Table 4. 16: Percentage calculation of ductile-brittle fracture areas in multi-layer welding at various temperatures with V and U grooves

Temperature (°C) / **Grooves**	MV	MU
	Area % of Ductile-Brittle Surface	

Room Temperature	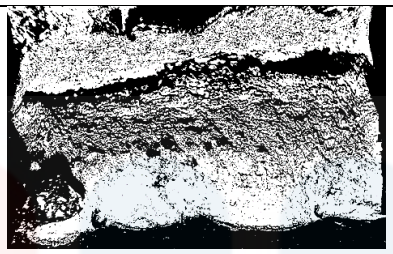 D= 51.83% B= 48.17%	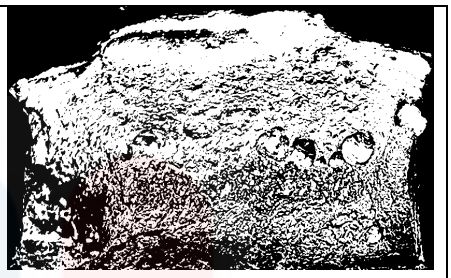 D= 52.09% B= 47.91%
0°C	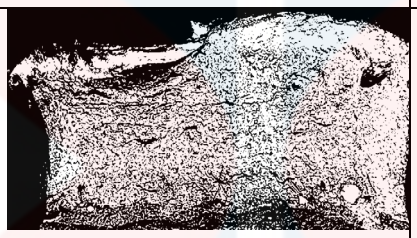 D= 51.61% B= 48.39%	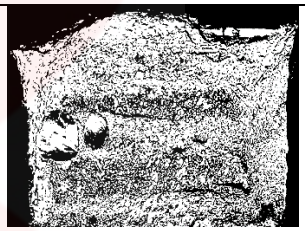 D= 54.04% B= 45.99%
-20°C	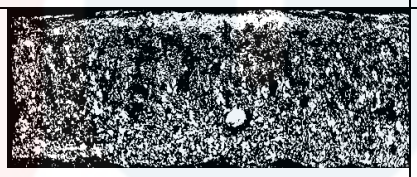 D= 35.95% B= 64.05%	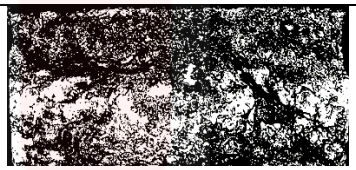 D= 36.20% B= 63.80%

In multi-layer welding, both V and U groove exhibit ductile behaviour at room temperature and 0°C. At room temperature, the ductile surface area exceeds the brittle surface which shows 51.83% for V groove and 52.09% for U groove. Similarly, at 0°C the ductile surface area was 51.61% for V groove and 54.04% for U groove while the remaining considered as brittle. However, at -20°C both MV and MU display brittle behaviour with high brittle surface area of 64.05% and 63.80% respectively. Notably, when compared to single layer welding the multi-layer welding for both grooves remains brittle even at -20°C due to a phenomenon known as cold embrittlement at lower temperatures. Additionally, multi-layer

welds show high toughness compared to single layer welding due to the multiple pass which allow for better fusion between adjacent layers.

CHAPTER 5

CONCLUSIONS AND RECOMMENDATIONS

5.1 Conclusions

At the end of this project, there were a few conclusions that could be made from the results and discussions in Chapter 4. Microstructure in SU reveals AF and PF while MV reveals the microstructure of polygonal ferrite. This reflected the groove shape affects the microstructure formation in both single and multi-layer welding. From the hardness test results, SU exhibited higher hardness than SV whereas MV exhibited higher hardness than MU. The results of impact toughness test for single layer welding at room temperature showed that no significance difference between SV and SU. However, SU demonstrated superior impact toughness compared to SV at 0°C while SV slightly advantage SU at -20°C. For multi-layer welding, MV consistently demonstrated superior impact toughness across both room temperature and 0°C. However, MU exhibited better impact toughness at -20°C compared to MV. The results from Vicker hardness test and Charpy impact test reflected the influence of groove shape on materials mechanical properties.

5.2 Recommendations

In future studies, there are a few recommendations that could be carried to obtain a better result. First, advance microscopy technique like Scanning Electron

Microscope (SEM) could be carried out to enhance microstructure analysis, providing high resolution imaging for a more detailed understanding of the material's properties. Second, duplicate or triplicate of samples for Vickers hardness testing to obtain average value for accurate results. Third, employing precise temperature measurement techniques such as using thermometer is essential to accurately monitor and control sample temperatures during impact test.

REFERENCES

Aldeeb, T., & Abduelmula, M. (2018). Fatigue strength of S275 mild steel under cyclic loading. *Interntional Journal of Materials and Metallurgical Engineering*, *12*(10) https://doi.org/10.5281/zenodo.1474960

Ali, M., Porter, D., Kömi, J., Eissa, M., El Faramawy, H., & Mattar, T. (2019). Effect of cooling rate and composition on microstructure and mechanical properties of ultrahigh-strength steels. *Journal of Iron and Steel Research International*, *26*(12), 1350–1365. https://doi.org/10.1007/s42243-019-00276-0

Anis, A. L., Talari, M. K., Mohd Arif, I. A., Kishore Babu, N., Ismail, M. H., & Janaki Ram, G. D. (2017). Microstructure and mechanical properties of Ti-15-3 alloy gas tungsten arc welds prepared using CP-Titanium filler. *Transactions of the Indian Institute of Metals*, *70*(3), 685–690. https://doi.org/10.1007/s12666-017-1049-2

Bodude, M. A., & Momohjimoh, I. (2015). Studies on effects of welding parameters on the mechanical properties of welded low-carbon steel. *Journal of Minerals and Materials Characterization and Engineering*, *03*(03), 142–153. https://doi.org/10.4236/jmmce.2015.33017

Bonnekoh, C., Jäntsch, U., Hoffmann, J., Leiste, H., Hartmaier, A., Weygand, D., Hoffmann, A., & Reiser, J. (2019). The brittle-to-ductile transition in cold rolled tungsten plates: Impact of crystallographic texture, grain size and dislocation density on the transition temperature. *International Journal of Refractory Metals and Hard Materials*, *78*, 146–163. https://doi.org/10.1016/j.ijrmhm.2018.09.010

Carlos, J., Guimarães, F., Matheus Campolina Mendes, de, I., Leonardo Sales Araújo, V.R. dos Santos, Rebello, A., & Evans, G. M. (2021). Microstructure characterization and its

relationship with impact toughness of C-Mn and high strength low alloy steel weld metals - A review. *Journal of Materials Research and Technology*, *10*, 471–501. https://doi.org/10.1016/j.jmrt.2020.12.006

Deepak, J. R., Bupesh Raja, V. K., Srikanth, D., Surendran, H., & Nickolas, M. M. (2021). non-destructive testing (NDT) techniques for low carbon steel welded joints: A review and experimental study. *Materials Today: Proceedings*, *44*, 3732–3737. https://doi.org/10.1016/j.matpr.2020.11.578

Dissertation, M., Bruno Alves Caio Supervisor, L., Martins Almeida Silva, A., & Alvarez Bestard, G. (2021). Analysis and estimation of extension of the fusion zone and sub-regions of the heat affected zone through neural networks in weld beads produced by GMAW Process. *University of Brasilia Mechanical Engineering Department.*

Ebrahimi, A., Babu, A., Kleijn, C. R., Hermans, M. J. M., & Richardson, I. M. (2021). The effect of groove shape on molten metal flow behaviour in gas metal arc welding. *Materials*, *14*(23). https://doi.org/10.3390/ma14237444

Ekaputra, I. M. W., Mungkasi, S., Dwi Haryadi, G., Tungga Dewa, R., & Kim, S. J. (2018). The influence of welding speed conditions of GMAW on mechanical properties of 316L austenitic stainless steel. *MATEC Web of Conferences*, *159*. https://doi.org/10.1051/matecconf/201815902009

Elfallah, S. S. S. (2022). Study on the influence of groove shape on the tensile strength of commercial steel. *Journal of Engineering Research*. https://doi.org/10.36909/jer.18695

Eroğlu, M., Aksoy, M., & Orhan, N. (1999). Effect of coarse initial grain size on microstructure and mechanical properties of weld metal and HAZ of a low carbon steel. *Materials Science and Engineering: A*, *269*(1-2), 59–66. https://doi.org/10.1016/s0921-5093(99)00137-9

Evans, R. (2012). Selection and testing of metalworking fluids. *Metalworking Fluids (MWFs) for Cutting and Grinding: Fundamentals and Recent Advances*, 23–78. https://doi.org/10.1533/9780857095305.23

Ghazvinloo, H., Honarbakhsh-Raouf, A., & Shadfar, N. (2021). A comprehensive study on the welded joints appearance in GMAW. *Journal of Materials and Environmental Science*, *12*(12), 1320-1331.

Hossein Zakerinia, A. Kermanpur, & A. Najafizadeh. (2009). Color metallography; A suitable method for characterization of martensite and bainite in multiphase steels. *International Journal ISSI*, *6*, 14–18.

Ibrahim, I. A., Mohamat, S. A., Amir, A., & Ghalib, A. (2012). The effect of gas metal arc welding (GMAW) processes on different welding parameters. *Procedia Engineering*, *41*, 1502–1506. https://doi.org/10.1016/j.proeng.2012.07.342

Ikram, A., & Chung, H. (2017). The effect of EN ratio and current on microstructural and mechanical properties of weld joined by AC-GMAW on square groove butt joints. *Applied Sciences (Switzerland)*, *7*(3). https://doi.org/10.3390/app7030261

Kah, P., & Martikainen, J. (2012). Current trends in welding processes and materials: improve in effectiveness. *Reviews on Advanced Materials Science*, *30*(2), 189–200. https://www.academia.edu/download/42694717/Current_trends_in_welding_processes_and_20160215-6744-1lmelv7.pdf

Khamari, B. K., Dash, S. S., Karak, S. K., & Biswal, B. B. (2020). Effect of welding parameters on mechanical and microstructural properties of GMAW and SMAW mild steel joints. *Ironmaking and Steelmaking*, *47*(8), 844–851. https://doi.org/10.1080/03019233.2019.1623592

Khorrami, M. S., Mostafaei, M. A., Pouraliakbar, H., & Kokabi, A. H. (2014). Study on microstructure and mechanical characteristics of low-carbon steel and ferritic stainless

steel joints. *Materials Science and Engineering: A, 608*, 35–45. https://doi.org/10.1016/j.msea.2014.04.065

Ko, K. K., Jang, J. H., Tiwari, S., Bae, H. J., Sung, H. K., Kim, J. G., & Seol, J. B. (2022). Quantitative analysis of retained austenite in Nb added Fe-based alloy. *Applied Microscopy*, *52*(1). https://doi.org/10.1186/s42649-022-00074-1

Kumar Gupta, S., Mehrotra, S., Ravi Raja, A., & Khan Yusufzai, M. (2019). Effect Of welding speed on weld bead geometry and percentage dilution in gas metal arc welding Of SS409L. *Materials Today: Proceedings*, 18. www.sciencedirect.comwww.materialstoday.com/proceedings2214-7853

Kumar, S., Singh, A., & Singh, G. (2017). Influence of current on microstructure and hardness of butt welding aluminium AA 6082 using GTAW process 1. *International Journal of Research in Mechanical Engineering and Technology, 3*(2).

Mansjur, Z., Sumual, H. M., & Tamba, I. P. (2019). The effect of groove welding on mechanical properties and microstructure of wear resistance steel plate by submerged arc welding. *IOP Conference Series: Materials Science and Engineering*, *694*(1). https://doi.org/10.1088/1757-899X/694/1/012027

Mao, G., Cao, R., Cayron, C., Mao, X., Logé, R., & Chen, J. (2019). Effect of cooling conditions on microstructures and mechanical behaviors of reheated low-carbon weld metals. *Materials Science and Engineering: A*, *744*, 671–681. https://doi.org/10.1016/j.msea.2018.12.035

Mendonça, R. R., Nogueira, I. M. S., Lovo, J. F. P., & Canale, L. C. F. (2020). Multiple etchings methodology: a new approach in multiphase steel characterization. *Journal of Microscopy*, *277*(2), 93–99. https://doi.org/10.1111/jmi.12871

Meseguer-Valdenebro, J. L., Martínez-Conesa, E., & Portoles, A. (2022). Influence of welding parameters on grain size, HAZ and degree of dilution of 6063-T5 alloy:

optimization through the Taguchi method of the GMAW process. *International Journal of Advanced Manufacturing Technology*, *120*(9–10), 6515–6529. https://doi.org/10.1007/s00170-022-09094-3

Mohanty, U. K., Abe, Y., Fujimoto, T., Nakatani, M., Kitagawa, A., Tanaka, M., Suga, T., & Sharma, A. (2020). Performance Evaluation of Alternating Current Square Waveform Submerged Arc Welding as a Candidate for Fabrication of Thick Welds in 2.25Cr-1Mo Heat-Resistant Steel. *Journal of Pressure Vessel Technology, Transactions of the ASME*, *142*(4). https://doi.org/10.1115/1.4046785

Moon, H. S., Kim, Y. B., & Beattie, R. J. (2006). Multi sensor data fusion for improving performance and reliability of fully automatic welding system. *International Journal of Advanced Manufacturing Technology*, *28*(3–4), 286–293. https://doi.org/10.1007/s00170-004-2359-1

Moore, P., & Booth, G. (2015). Mechanical testing of welds. *The Welding Engineers Guide to Fracture and Fatigue*, 113–141. https://doi.org/10.1533/9781782423911.2.113

Mvola, B., & Kah, P. (2017). Effects of shielding gas control: welded joint properties in GMAW process optimization. *International Journal of Advanced Manufacturing Technology*, *88*(9–12), 2369–2387. https://doi.org/10.1007/S00170-016-8936-2

Naidu, D. S., Ozcelik, S., & Moore, K. L. (2003). Gas Metal Arc Welding: Modeling. *Modeling, Sensing and Control of Gas Metal Arc Welding*, 9–93. https://doi.org/10.1016/B978-008044066-8/50004-5

Olabode, M., Kah, P., & Martikainen, J. (2013). Aluminium alloys welding processes: Challenges, joint types and process selection. *Proceedings of the Institution of Mechanical Engineers, Part B: Journal of Engineering Manufacture*, *227*(8), 1129–1137. https://doi.org/10.1177/0954405413484015

Parmar, G., Pathak, A. K., & Khan, M. R. (2021). A Study of Mechanical Properties of MIG Welding and TIG Welding Welded Dissimilar Joint of Mild Steel and 304 Austenitic Stainless Steel. *International Research Journal of Engineering and Technology 8*(4).

Pathak, D., Singh, R. P., Gaur, S., & Balu, V. (2020). Influence of groove angle on hardness and reinforcement height of shielded metal arc welded joints for low carbon AISI 1016 steel plates. *Materials Today: Proceedings*, *38*, 40–43. https://doi.org/10.1016/j.matpr.2020.05.597

Posch, G., Scherleitner, W., Rutzinger, B., Schmitt, G., Kamath, V., & Fiedler, M. (2014). Manufacturing of nickelbase-overlays: Comparison of various welding technologies under consideration of clad properties. *IIW International Congress IC*.

Sarolkar, A. D., & Kolhe, K. P. (2017). Effect of process parameters on weld bead geometry and micro-hardness of welding AA 6082 using GTAW process. *Journal of Emerging Technologies and Innovative Research, 4*(10).

Sattari-Far, I., & Farahani, M. R. (2009). Effect of the weld groove shape and pass number on residual stresses in butt-welded pipes. *International Journal of Pressure Vessels and Piping*, *86*(11), 723–731. https://doi.org/10.1016/j.ijpvp.2009.07.007

Sharma, V., & Shahi, A. S. (2014). Effect of groove design on mechanical and metallurgical properties of quenched and tempered low alloy abrasion resistant steel welded joints. *Materials and Design*, *53*, 727–736. https://doi.org/10.1016/j.matdes.2013.07.043

Singh, M., Shahi, A. S., & Singh, D. (2020). Effect of weld groove volume on the mechanical and metallurgical performance of GTA welded martensitic stainless steel (AISI 410 SS) joints. *Materials Today: Proceedings*, *28*, 1580–1587. https://doi.org/10.1016/j.matpr.2020.04.844

Singh, R. (2020). Physics of Welding. *Applied Welding Engineering*, 125–155. https://doi.org/10.1016/b978-0-12-391916-8.00014-5

Singh, T., Singh, A., & Saini, S. (2019). Effect of groove design on the mechanical properties of shielded metal arc welded joints. *Indian Journal of Science and Technology*, *12*(2), 1–8. https://doi.org/10.17485/ijst/2019/v12i2/139920

Śloderbach, Z., & Pajak, J. (2015). Determination of ranges of components of heat affected zone including changes of structure. *Archives of Metallurgy and Materials 60(*4). https://doi.org/10.1515/amm-2015-0421

Sultana, M., Hasan, M. F., & Islam, M. (2014). Analysis of mechanical properties of mild steel applying various heat treatment. *International Conference on Mechanical, Industrial and Energy Engineering*, 25-26.

Wang, Y., Zhang, Y., Godfrey, A., Kang, J., Peng, Y., Wang, T., Hansen, N., & Huang, X. (2021). Cryogenic toughness in a low-cost austenitic steel. *Communications Materials*, *2*(1). https://doi.org/10.1038/s43246-021-00149-8

Waqas, A., Qin, X., Xiong, J., Zheng, C., & Wang, H. (2019). Analysis of ductile fracture obtained by charpy impact test of a steel structure created by robot-assisted GMAW-based additive manufacturing. *Metals*, *9*(11). https://doi.org/10.3390/met9111208

Winarto, W., Oktadinata, H., & Siradj, E. S. (2018). Microstructure and Hardness Properties of Butt and Fillet GMAW Welded Joints on HY80 High Strength Steel Plate. *AIP Conference Proceedings*, *1977*. https://doi.org/10.1063/1.5046656

Xiao, H., Zheng, S., Xin, Y., Xu, J., Han, K., Li, H., & Zhai, Q. (2020). Characterization of microstructure in high-hardness surface layer of low-carbon steel. *Metals*, *10*(8), 1–10. https://doi.org/10.3390/met10080995

Ye, Y., Cai, J., Jiang, X., Dai, D., & Deng, D. (2015). Influence of groove type on welding-induced residual stress, deformation and width of sensitization region in a SUS304 steel butt welded joint. *Advances in Engineering Software, 86,* 39-48. https://doi.org/10.1016/j.advengsoft.2015.04.001

Zaidi, A., & Madavi, K. R. (2018). Improvement of welding penetration in MIG welding. *International Journal of Research in Science and Technology, 4*(5), 1198-1203.

Zhao, Y., Tong, X., Wei, X. H., Xu, S. S., Lan, S., Wang, X. L., & Zhang, Z. W. (2019). Effects of microstructure on crack resistance and low-temperature toughness of ultra-low carbon high strength steel. *International Journal of Plasticity*, *116*, 203–215. https://doi.org/10.1016/j.ijplas.2019.01.004

APPENDIX A

Figure A1: Welding safety equipment

Figure A2: Argon gas

Figure A3: Hardness value for single layer V and U groove

	Hardness Value (HV)

Point	SV	SU
1	187	189
2	219	217
3	219	236
4	227	189
5	224	248
6	238	260
7	242	241
8	239	230
9	232	227
10	229	221
11	165	198

Figure A4: Hardness value for multi-layer V and U groove

Point	Hardness Value (HV)	
	MV	MU
1	157	168
2	169	178
3	186	201
4	200	207
5	211	226
6	255	223
7	239	205
8	225	200

9	215	194
10	205	181
11	156	165